Curvature of Synthetic and Natural Surfaces Is an Important Target Feature in Classical Pathway Complement Activation

Martin Bjerregård Pedersen, Xingfei Zhou, Esben Kjær Unmack Larsen, Uffe Skov Sørensen, Jørgen Kjems, Jens Vinge Nygaard, Jens Randel Nyengaard, Rikke Louise Meyer, Thomas Boesen and Thomas Vorup-Jensen

J Immunol 2010; 184:1931-1945; Prepublished online 6 January 2010;
doi: 10.4049/jimmunol.0902214
http://www.jimmunol.org/content/184/4/1931

The Journal of Immunology is published twice each month by
The American Association of Immunologists, Inc.,
9650 Rockville Pike, Bethesda, MD 20814-3994.

Print ISSN: 0022-1767 Online ISSN: 1550-6606.

Curvature of Synthetic and Natural Surfaces Is an Important Target Feature in Classical Pathway Complement Activation

Martin Bjerregård Pedersen,*,† Xingfei Zhou,* Esben Kjær Unmack Larsen,* Uffe Skov Sørensen,‡ Jørgen Kjems,* Jens Vinge Nygaard,* Jens Randel Nyengaard,§ Rikke Louise Meyer,* Thomas Boesen,¶ and Thomas Vorup-Jensen*,†,‡

The binding of Abs to microbial surfaces followed by complement activation constitutes an important line of defense against infections. In this study, we have investigated the relationship between complement activation and the binding of human IgM Abs to surfaces with different curvatures. IgM Abs to dextran were shown to activate complement potently on dextran-coated particles having a diameter around 250 nm, whereas larger (600 nm) particles were less potent activators. This selectivity regarding particle dimension was also found for complement activation by colloidal substances of microbial origin. Peptidoglycan (PGN) is the major chemical component in the cell wall of Gram-positive bacteria. Fragments of purified PGN with sizes of ~100 nm promoted complement activation effectively through the classical pathway. By contrast, larger or smaller fragments of PGN did not activate complement strongly. A careful analysis of PGN fragments released during planctonic growth of *Staphylococcus aureus* showed that these include curvatures that would permit strong IgM-mediated complement activation, whereas the curvature of intact cells would be less effective for such activation. Consistently, we found that the suspended PGN fragments were strong activators of complement through the classical pathway. We suggest that these fragments act as decoy targets for complement activation, providing protection for *S. aureus* against the host immune response to infection. ***The Journal of Immunology*****, 2010, 184: 1931–1945.**

An important part of immunity to infections consists of plasma proteins that are deposited on the surface of invading microbes to facilitate their elimination by phagocytic cells. The complement system comprises more than 30 proteins that are either directly deposited on microbial target surfaces or participate in regulating the deposition (1). Complement activation proceeds through the classical, lectin, and alternative pathways. Activation through the classical pathway is initiated by the binding of the C1 complex to Abs on the microbial surface. The lectin pathway of complement activation is initiated by binding of mannan-binding lectin (MBL) to carbohydrates exposed by microbes. Both the classical and lectin pathways lead to the deposition of a proteolytic fragment of C3 on the target surface; this deposition may also proceed through the alternative pathway with the spontaneous formation of a covalent bond between C3 and hydroxyl or amine groups on the microbial molecules. In terms of defining the molecular mechanisms that keep soluble complement factors in their unactivated state and allow for activation only upon binding of the factors to target surfaces, several structural investigations now suggest that conformational changes are important (2–5). According to a recent experimental study, the binding of MBL to ligand-coated surfaces stretches the lectin molecule (2), and a similar mechanism was suggested for binding of the C1 complex to Ab-coated targets, where this change supports activation of the associated C1r and C1s proteases (4).

Small molecular structures critically determine how the immune system distinguishes self from nonself to protect against infections, and epitope recognition by Abs typically involves a buried surface of 12–20 nm^2 (6). However, in the case of large Igs such as soluble IgM, the binding between the molecule and the epitope-presenting surface involves structural features over an area far larger than the interface between a single paratope and epitope. The IgM molecule usually consists of five to six monomeric subunits in plasma, based on interacting N-terminal heavy and L chain variable domains (V_H and V_L) followed by four constant H chain domains (Cμ) in the H chain. The subunits are linked covalently through a joining (J) chain and small angle x-ray scattering studies of pentameric IgM (7) revealed a planar and symmetrical structure of the five monomeric units with the Fc portions of the monomers forming a central disk (Fc_5) with protruding $F(ab')_2$ arms (8). The Cμ1 domains in the Fab fragments are connected to the Fc_5/J chain disc through a linker region represented by the Cμ2 domain. As shown by Feinstein et al. (9, 10), IgM bound to a bacterial flagellum permitted the $F(ab')_2$ arms to bend toward the Ag-presenting surface in a staple-like conformation. Based on their small angle x-ray scattering studies, Perkins et al. (7) suggested that the bending of Fab fragments at an angle of ~60° relative to the plane of Fc_5 disc exposes a binding site for C1q in the Cμ2 domains [which is part of $F(ab')_2$ but not of Fab] of IgM. In solution, human IgM has a radius of gyration of 12 nm and a maximum dimension of 35–37 nm in good agreement with the cross-sectional diameter estimated from transmission electron microscopy (TEM) (7, 8). Topological features,

*Interdisciplinary Nanoscience Center, †Biophysical Immunology Laboratory, ‡Department of Medical Microbiology and Immunology, §Stereology and Electron Microscopy Research Laboratory and MIND Center, and ¶Department of Molecular Biology, Center for Carbohydrate Recognition and Signalling, University of Aarhus, Aarhus, Denmark

Received for publication July 13, 2009. Accepted for publication December 3, 2009.

This work was supported by a stipend from the Danish Medical Research Council to M.B.P. (271-06-0121) and grants from the Danish Science Research Council, Danish Council for Strategic Research, LEO Pharma Foundation, The Beckett Foundation, The Oticon Foundation, and Consul Johannes Fogh Nielsens Legat.

Address correspondence and reprint requests to Dr. Thomas Vorup-Jensen, Department of Medical Microbiology and Immunology, University of Aarhus, The Bartholin Building (Building 1240), Wilhelm Meyers Alle, DK-8000 Aarhus C, Denmark. E-mail address: vorup-jensen@microbiology.au.dk

Abbreviations used in this paper: AFM, atomic force microscopy; CCHA, consumption of complement hemolytic activity; CHA, complement hemolytic activity; CV, coefficient of variation; DLS, dynamic light scattering; E, erythrocyte; GVB, gelatin/veronal-buffered saline; J, joining; MBL, mannan-binding lectin; PGN, peptidoglycan; RRBC, rabbit RBC; TBS/Tw, Tween-20 in TBS; TEM, transmission electron microscopy; TRIFMA, time-resolved immunofluorometric assay.

www.jimmunol.org/cgi/doi/10.4049/jimmunol.0902214

including curvature or epitope density, are likely to affect the conformation of surface-bound IgM. However, the influence of surface topology in regulating the effector functions of IgM, such as complement activation, has not been studied.

The Gram-positive bacterium *Staphylococcus aureus* is an important human pathogen and causes both community-acquired and nosocomial infections. Peptidoglycan (PGN) is the major component in the cell walls of Gram-positive bacteria and forms a highly complex structure, which is critical for the shape and size properties of the bacteria (11). The backbone in the PGN polymer consists of glucan strands of repeating disaccharide units of *N*-acetyl-D-glucosamine–(β-1,4)-*N*-acetylmuramic acid, where the muramic acid moiety is linked to a stem peptide of four or five alternating L- and D-amino acids. These disaccharide-peptide units are cross-linked by interpeptide bridges, resulting in a rigid mesh-like structure. The PGN layer is highly dynamic and constantly remodeled during cell growth through enzymatic processes (12). The role of PGN in stimulating the immune system is well established (13, 14), and PGN is the major source of complement-activating macromolecules produced by *S. aureus* (15). Furthermore, IgG and IgM Abs to PGN are frequently found in normal individuals (16). The continuous remodeling of the cell wall is likely to liberate material that activates the immune response against *S. aureus*, but whether cell wall fragmentation plays a distinct role in this process remains unclear. Interestingly, experiments show that enzymatically degraded PGN is a more potent activator of the complement system than intact PGN (17), but the molecular rationale for this observation has not been characterized.

In this study, we have investigated the role of topological features of surfaces in complement activation. By use of nanoparticles coated with dextran Ag, we show that the size and hence the curvature of the particles is a key parameter for determining the ability of large Igs such as IgM to initiate complement activation through the classical pathway. These considerations led us to investigate whether microbial surface topology also regulates complement activation, and we report in this paper that the curvature of PGN layers influences activation through the classical pathway in a similar manner to the Ag-coated nanoparticles. During planctonic growth and death, *S. aureus* liberates fragments of the cell wall into the culture medium. Compared to the relatively flat surface of intact bacteria, the sharper curvature of these PGN fragments apparently makes them stronger activators of complement.

Materials and Methods

Human sera

Human sera were obtained from the local blood bank (Department of Clinical Immunology, Aarhus University Hospital, Skejby, Denmark) and made available to the project according to procedures approved by the local scientific ethics committee. For each serum, the concentration of MBL was determined by a previously described assay (18). Testing of the C3 concentration in serum from Donor 1 was carried out by a standard clinical assay (complement C3c version 2, Tina-quant; Roche Diagnostics, Basel, Switzerland).

Hemolytic assays for complement activation by dextran-coated nanoparticles

Nanoparticles with an iron oxide core surrounded by a stabilizing layer of dextran (fluidMAG-DX, catalog number 4104) or carboxymethyl-dextran (fluidMAG-CMX, catalog number 4106) with hydrodynamic diameters of 50 nm, 100 nm, and 250 nm were purchased from Chemicell (Berlin, Germany). Dextran-coated iron oxide beads with a diameter of ~600 nm (screenBEAD/R-DX) were a kind gift from Christian Bergemann and Dr. W. Rainer Quass (Chemicell).

Complement activation by nanoparticles was investigated in gelatin/veronal-buffered saline (GVB; 0.1% weight to volume ratio [w/v] gelatin, 0.1% [w/v] veronal, 140 mM NaCl; pH 7.4) with 1 mM $MgCl_2$ and 1 mM $CaCl_2$ (GVB/Mg^{2+}/Ca^{2+}). Suspensions of 400 μl were made with the fluidMAG-DX or fluidMAG-CMX nanoparticles such that the total calculated particle surface area was 5×10^{14} nm^2 for each size of particle as calculated from the formula

$$A_{Tot} = 4\pi \cdot (d/2)^2 \cdot n_{\text{particles}}, \quad (1)$$

where d is the particle diameter and $n_{\text{particles}}$ the total number of particles in suspension. Each nanoparticle suspension was mixed with human serum to a final serum concentration of 33% (v/v) in a total reaction volume of 600 μl. The serum/nanoparticle suspensions were incubated without further dilution as well as in suspension with 2-fold serial dilutions of the initial nanoparticle concentration at 37°C for 30 min with vigorous shaking to facilitate the activation of the complement system and consumption of active C3.

To estimate the complement activation induced by the nanoparticles, the residual complement-mediated hemolytic activity was estimated. Complement-mediated lysis of unsensitized rabbit RBCs (RRBCs) by human serum was quantified by a modified assay as described elsewhere (19). Rabbit blood was collected from the ear vein into tubes with a citrate/phosphate/dextrose/adenine solution (030603,Vacuette; Greiner bio-one, Kremsmuenster, Austria). RRBCs were isolated by centrifugation at 400 × *g* and washed three times in GVB prior to use, and the number of RRBC per ml was counted in a hemocytometer (Bürker-Türk, Marienfeld, Germany). A volume of 300 μl of GVB with 1 mM $MgCl_2$ and 20 mM EGTA (GVB/Mg^{2+}/EGTA) was added to each sample tube (20). Samples were centrifuged at 1740 × *g* for 10 min at 4°C to pellet the particles. A total of 100 μl supernatant from the centrifuged serum/nanoparticle suspensions and 50 μl RRBC suspension (~2×10^8 RRBC/ml) were incubated with agitation for 60 min at 37°C to yield hemolysis of the erythrocytes (Es) by the remaining unconsumed complement proteins in the nanoparticle-treated serum. The reactions were terminated by adding 1.2 ml ice-cold 0.9% (w/v) NaCl solution to each sample. The samples were centrifuged at 1250 × *g* for 10 min to pellet debris and intact RRBCs, and 200 μl of each supernatant was transferred to wells in a flat-bottomed microtiter plate for measurement of the OD at 405 nm. Zymosan from *Saccharomyces cerevisiae* (Z-4250, Sigma-Aldrich, St. Louis, MO) was used as a positive control for particle-induced complement activation (21) and treated similarly to the nanoparticles. The level of spontaneous lysis (OD_{sp}) of the RRBCs was tested by a sample of 50 μl RRBC suspension added to 100 μl GVB/Mg^{2+}/EGTA; as a measure of the OD at 100% lysis ($OD_{100\%}$), samples were made of 50 μl RRBC suspension added to 100 μl water. The residual complement hemolytic activity (CHA) in the serum samples was calculated as:

$$CHA = 100\% \cdot \frac{OD - OD_{sp}}{OD_{100\%} - OD_{sp}}. \quad (2)$$

A correction for the activation of complement during the incubation of serum not depending on the presence of nanoparticles was carried out by normalizing CHA values for serum incubated with nanoparticles ($CHA_{\text{nanoparticles}}$) to the CHA value for serum incubated without nanoparticles (CHA_0). This procedure also corrects the contribution from serum to the OD compared with the reference samples not containing serum (i.e., the spontaneous lysis of Es in GVB buffer and 100% lysis obtained by suspension of Es in water). Furthermore, to obtain a positive correlation with the assays measuring the generation of C3a-des Arg described below, the complement activation measured by hemolysis was expressed as consumption of CHA (CCHA):

$$CCHA = 100\% - 100\% \cdot \frac{CHA_{\text{nanoparticles}}}{CHA_0} \cdot \quad (3)$$

In experiments quantifying the role of the alternative pathway of complement activation, serum and nanoparticles were diluted in GVB/Mg^{2+}/EGTA buffer and incubated at 37°C for 30 min. As a control, the consumption of hemolytic activity by nanoparticles was tested in the presence of EDTA; samples of serum and nanoparticles were diluted in GVB with 1 mM EDTA followed by measuring of the residual hemolysis as described above.

Monodispersity and size of particles following complement activation

Following reactions to establish complement deposition on the surfaces of the applied nanoparticles, the size distribution of the particulate material was investigated by dynamic light scattering (DLS) (22). Measurements were performed on the particle suspensions with a Nano ZS instrument (Malvern Instruments, Malvern, U.K.), illuminating the sample with helium-neon laser

light (wavelength 633 nm) and a single photon-counting photodiode for signal detection. The autocorrelation was performed by the 5000/EPP photon correlator (ALV, Langen, Germany) and analyzed using Dispersion Technology Software (Malvern Instruments). In brief, the size distribution was obtained from the distribution in diffusion coefficients (D) (22), which are related to the hydrodynamic diameter of the particles (d_H) through the Stokes-Einstein equation:

$$d_H = \frac{kT}{3\pi\eta \cdot D}, \quad (4)$$

where k is the Boltzmann constant (1.38×10^{-23} J/K), η is the diluent viscosity (at 0.894×10^{-3} Pa/s for water), and T is the absolute temperature (298 K). Size measurements were made on 0.6-ml particle suspensions in plastic cuvettes (67742, Sarstedt, Nürnbrecht, Germany) at 25°C and repeated three times.

C3a-des Arg ELISA for measurement of complement activation by dextran-coated nanoparticles

For testing the C3a-des Arg generation, dextran-coated iron-oxide nanoparticles with diameters of 50 nm, 250 nm, and 600 nm were used. The particles were applied in amounts corresponding to a total surface area of 5×10^{14} nm^2 in GVB/Mg^{2+}/Ca^{2+} buffer with 33% (v/v) serum and incubated under conditions corresponding to those for the hemolytic assay. C3a-des Arg was measured with a commercially available kit (C3a EIA kit, Quidel, San Diego, CA). Following incubation, the samples were diluted 1,000–50,000-fold in sample buffer (Quidel) and applied to wells in the prefabricated microtiter strips coated with a murine mAb specific for human C3a-des Arg. Together with the application of standards and controls provided with the kit, the assay was carried out according to the manufacturer's instructions.

Similar assays were performed using polystyrene nanoparticles with diameters of 50 nm, 100 nm, 400 nm, 600 nm, and 800 nm (G. Kisker, Steinfurt, Germany). Polystyrene nanoparticles with a total surface area of 10^{16} nm^2 were coated with dextran by adding the particles to a solution of 10 mg/ml dextran in water (dextran from *Leuconostoc mesenteroides* with an M_r of 8,500–11,500; D9260, Sigma-Aldrich) followed by incubation at room temperature for 20 h. In the experiments with complement activation, the samples were diluted 20-fold in GVB/Mg^{2+}/Ca^{2+} to give a total surface area of 5×10^{14} nm^2. Complement activation was carried out as for the iron oxide particles.

Measurement of the binding activity of anti-dextran and anti-PGN Abs in donor sera

Donor sera were analyzed for the presence of anti-dextran Abs by a time-resolved immunofluorometric assay (TRIFMA). The assay was carried out in 96-well microtiter plates (FluoroNunc Maxisorb; Nunc, Kamstrup, Denmark) coated with dextran (M_r ~500,000) from *L. mesenteroides* (Sigma-Aldrich). The coating of the microtiter wells was carried out as previously described (23); solutions with 10 μg/ml dextran in Na_2CO_3/$NaHCO_3$ (pH 9.6) were applied in a volume of 100 μl. The plates were incubated overnight at 4°C and blocked by adding 200 μl per well of 1 mg/ml human serum albumin (Octalbin 20%, Octapharma AB, Stockholm, Sweden) in 140 mM NaCl and 10 mM Tris-HCl (pH 7.4) (TBS) followed by incubation for 60 min at 37°C. The plates were washed three times in 0.05% (v/v) Tween-20 in TBS (TBS/Tw). Each well received 100 μl serum sample diluted in TBS with 1 mM $CaCl_2$ (TBS/Ca^{2+}) to concentrations between 0.003% and 50% (v/v) followed by incubation for 1 to 2 h at room temperature in a humidified chamber. The wells were washed three times in TBS/Tw and incubated for 60 min with 100 μl biotinylated mAb to human IgM (clone HB57, Leinco Technologies, Ballwin, MO) or IgG (clone HP-6017, Sigma-Aldrich), each at a concentration of 1 μg/ml in TBS. The isotypic (IgG1) mAb KIM185 directed to an irrelevant Ag (human CD18) made locally from a hybridoma cell line bought from American Type Culture Collection (LGC Promochem, Boras, Sweden) was used as a control. After washing three times with TBS/Tw, 100 μl of 0.1 μg/ml europium-labeled streptavidin (PerkinElmer, Waltham, MA) in TBS/Tw containing 25 μM EDTA was added to each well and incubated for 1 h at room temperature. TRIFMA was performed as described elsewhere using a VICTOR 3 1420 multilabel counter (PerkinElmer).

Donor sera were analyzed for PGN-reactive IgM and IgG Abs in a procedure similar to the analysis for dextran-reactive Abs. Lyophilized PGN from *S. aureus* (77140, Sigma-Aldrich) was suspended at a concentration of 1 mg/ml in PBS buffer (pH 7.4). Suspensions of 6 ml were sonicated for 20 min at 40 W with a Sonifier B-12 (Branson, Danbury, CT) ultrasound probe to obtain a relatively monodisperse suspension of PGN particles. The sonicated PGN was diluted in Na_2CO_3/$NaHCO_3$ buffer (pH 9.6) at a concentration of 10 μg/ml and applied to microtiter wells; coating and washing of the plates was carried out as described for the dextran assay. Serum samples were added in a dilution range from 0.001% (v/v) as well as in further 3-fold serial dilutions for IgG measurements and 50% (v/v) and in further 3-fold serial dilutions for the IgM measurements. The amount of bound Ig was tested by TRIFMA as described above.

Binding of IgM and IgG to dextran-coated nanoparticles

The binding of IgM and IgG to 250-nm and 600-nm dextran-coated fluidMAG (Chemicell) particles was investigated with a modified TRIFMA. Nanoparticles with a total particle surface area of 5×10^{14} nm^2 in TBS/Tw/Ca^{2+} with 33% (v/v) serum were incubated at 37°C for 30 min with agitation. The suspensions were made in 1.5-ml tubes preblocked by incubation at 4°C for ~16 h with 1.2 ml of 1 mg/ml human serum albumin (Octapharma AB) in TBS. The 250-nm particles were washed twice in TBS/Tw/Ca^{2+} buffer by collecting the particles with a magnet (Dynal MPC-S, catalog number 120.20D; Invitrogen Dynal AS, Oslo, Norway). The nonmagnetic 600-nm particles were collected by centrifugation at $700 \times g$ for 2 min and washed twice. Biotinylated mAbs to human IgM (clone HB57) or IgG (clone HP-6017), or, as isotypic control, KIM-185 diluted to 1 μg/ml in TBS were added to the beads and incubated for 60 min at room temperature. The particles were washed two times in TBS/Tw/Ca^{2+} followed by addition of 0.1 μg/ml europium-labeled streptavidin in TBS/Tw with 25 μM EDTA to each tube and incubation for 1 h at room temperature. The particles were washed two times in TBS/Tw/Ca^{2+}. Enhancement buffer with 0.57% (v/v) acetic acid, 0.1% (v/v) Triton X-100, 1% (w/v) PEG_{6000}, 15 μM 2-naphtoyltrifluoroacetone, and 50 μM Tris (*n*-octyl) phosphine oxide (pH 3.2) was added (400 μl per tube) followed by vigorous shaking of the tubes for 5 min. The particles were separated from the supernatant, which was loaded into a flat-bottomed microtiter plate for reading of the fluorescence signal as described above.

Analysis of complement activation by particulate material from purified S. aureus *PGN*

Aliquots of the sonicated PGN, prepared as described above, were treated with either 0.5 μg/ml lysostaphin (Sigma-Aldrich) or 0.5 μg/ml lysostaphin and 3 U mutanolysin (M9901, Sigma-Aldrich) per 100 μg PGN (17). The samples were incubated for 110 min at 37°C. The PGN preparations were immediately frozen on an ethanol/dry-ice bath and stored at −80°C. The size distribution of the particulate material was analyzed by DLS as described for the iron oxide particles. The PGN suspension was mixed with human serum from Donor 1 or either of two C1q deficient sera (catalog number C8567, Sigma-Aldrich, or catalog number A509, Quidel) to a final serum concentration of 33% (v/v) and a final PGN concentration of 20 μg/ml in a total reaction volume of 600 μl. The serum/PGN suspensions were incubated at 37°C for 30 min with vigorous shaking, permitting the activation of the complement system and consumption of active C3. Complement activation was tested in GVB/Mg^{2+}/Ca^{2+} or GVB/Mg^{2+}/EGTA buffer. Further controls were made by testing the activation with dilutions of lysostaphin or mutanolysin in the absence of PGN.

Microscopic analysis of S. aureus *debris*

Todd-Hewitt medium (Oxoid, Basingstoke, U.K.) was filtered through a sterile filter (0.22 μm), which, prior to use, was rinsed in distilled water. Small scale cultures (~3 ml) of the medium were inoculated with the *S. aureus* strain T7 (24) and incubated for ~16 h at 37°C. Samples of fixed bacteria were made by mixing 0.5 ml bacterial culture with 1.5 ml paraformaldehyde followed by incubation for 2 h at room temperature. The sample was rinsed twice in PBS, resuspended in PBS with 50% (v/v) ethanol, and stored at −20°C. A small volume (20 μl) of the suspension of fixed *S. aureus* was placed on polylysine-coated microscope slides (Polysine, J2800AMNZ; Menzel-Gläser, Braunschweig, Germany); the roughness of the surface was 5 nm. The sample was incubated for 15 min at ambient conditions followed by rinsing in PBS buffer (pH 7.4) and drying with a stream of N_2 gas. All measurements were carried out with a JPK NanoWizardII (JPK Instruments, Berlin, Germany) atomic force microscope (AFM) mounted on an inverted optical microscope (Axiovert 200M, Carl Zeiss Microimaging, Jena, Germany). Imaging in air was performed in the intermittent contact mode to reduce the tip-sample interaction and the lateral forces. The silicon probes (RTESP; Veeco, Santa Barbara, CA) used for imaging had a nominal spring constant of 40 N/m and nominal resonance frequency of ~300 kHz.

For TEM imaging of fragments released from *S. aureus* during culture, a filtrate of the culture medium was made following the growth of bacteria as

described above. The medium was passed through a sterile filter (0.22 μm), and NaN_3 was added to a final concentration of 0.01% (w/v). Samples of the filtrate were incubated either with 0.5 μg/ml lysostaphin (L4402, Sigma-Aldrich) or 16 μg/ml trypsin (S2012, DakoCytomation, Glostrup, Copenhagen) for 16 h at 37˚C. Specimens for TEM were made essentially as described earlier (25). A suspension of 3% (w/v) low-melting agarose (50111, Sea-Plaque GTG Agarose, FME, Rockland, ME) in water was heated until the agarose melted and then kept liquefied at 40˚C in a water bath. Samples, heated at 40˚C, of either untreated filtrate or filtrate treated with lysostaphin or trypsin was mixed with the liquid agarose solution to a final agarose concentration of 1% (w/v), and the specimens were allowed to solidify. The agarose-supported culture filtrates were fixed with PBS-buffered 2% (v/v) glutaraldehyde and transferred into PBS with 75 mM sucrose (pH 7.3). The samples were refixed in 1% (w/v) OsO_4 and transferred into 50 mM maleic acid (pH 5.2), then dehydrated with a graded series of alcohols before embedding in epoxy resin (Epon, TAAB Laboratories Equipment, Berkshire, U.K.). Sections with a thickness of ~60 nm were cut with an RMC MT-XL ultramicrotome (Boeckeler Instruments, Tucson, AZ) and visualized on a Philips CM10 transmission electron microscope (Philips, Eindhoven, The Netherlands) with a Kodak Megaplus model 1.6i camera (Kodak, Rochester, NY) connected to a PC with iTEM software version 5 (Olympus Soft Imaging Solutions, Münster, Germany).

Quantification of the curvature of the S. aureus *PGN fragments*

The grayscaled TEM image of PGN fragments liberated from cultured *S. aureus* into culture medium was analyzed with the MatLab software package (MathWorks, Natick, MA) using the image processing toolbox DipImage v. 6.3. Uneven illumination of the image during TEM acquisition was corrected by applying a high-pass filter. Further preparations for analysis were made by removing all pixels closer than 75 nm to the border of the image. PGN fragments within the image were then separated from the background by setting a threshold and assigning a value of either zero or one to each pixel in the image. This network of PGN fragments were then further identified as thin lines of neighboring pixels with values at one. The network was broken into individual fragments by removing single pixels located at network nodes. Following an exclusion of all fragments <35 nm, a total of 101 individual fragments were included in the curvature analysis. The path of each fragment described by a thin line of pixels was approximated by a polynomium to obtain a continuous curve from which the curvature along the path was calculated. From the definition (26, 27) of curvature, κ, it follows that the curvature at each pixel point along the path is equivalent to the reciprocal radius according to Equation 5:

$$\kappa = \frac{1}{r} = \frac{2}{d}, \qquad (5)$$

where r is the radius and d the diameter, respectively, of a circle located with the path as its tangent. The distribution of the mean curvature of all 101 fragments was analyzed by using a probe consisting of a segment of the curve with a length of 35 nm (i.e., corresponding to the cross-sectional diameter of IgM). The probe was moved along each fragment in increments of one pixel (1.2 nm), and the mean curvature over the length of the probe, $<\kappa>_{35\ nm}$, was calculated. The distribution of $<\kappa>_{35\ nm}$ was calculated over the range from 0.01 nm^{-1} to 0.99 nm^{-1} by grouping the values of $<\kappa>_{35\ nm}$ into intervals of 0.01 nm^{-1} and calculating for each interval the frequency of $<\kappa>_{35\ nm}$ in that interval.

Statistical analyses

All statistical comparisons were made by nonparametric methods. Comparisons between groups were carried out by a Kruskal-Wallis analysis with Dunn's correction for multiple comparisons. The correlation between Ig binding activities to dextran for the eight donor sera to dextran and complement activation by the nanoparticles was analyzed by nonparametric statistics using Spearman's rank order correlation method. All calculations were made with GraphPad Prism version 5 (GraphPad, San Diego, CA).

Results

Complement activation by dextran-coated nanoparticles with different curvatures

Several studies have shown that nanoparticles with appropriate surface coating may activate the complement system as typically monitored by hemolysis assays (28–30). Particles with diameters of 50–100 nm are comparable in size to the larger molecules of the complement system (i.e., C1q and MBL, as well as IgM). Consequently, we surmised that perturbations in the functions of these molecules would be noticeable when changes were made to the size of particles spanning this size range. The well-defined shape and size of iron oxide nanoparticles (31) make them an attractive choice for studying the influence of surface topology in the activation of the complement system. Specifically, the spherical shape of the particles reduces the topological parameters characterizing the surfaces to only one, namely the curvature, which is a strict function of the diameter.

To understand the possible relationship between the topology of surfaces and their ability to activate the complement system, we decided to test iron oxide particles coated with dextran. These were mixed with serum from Donor 1 and incubated under conditions permitting complement activation through all pathways (i.e., in the presence of Mg^{2+} and Ca^{2+}) (Fig. 1*A*), or under conditions favoring complement activation through the alternative pathway (i.e., in the presence of Mg^{2+} and EGTA) (Fig. 1*B*). Particles with diameters of 50, 250, and 600 nm were added to the serum and the complement activation by the particles was measured in a hemolytic assay as the CCHA. The particle-induced complement activation was determined by comparison with a sample of donor serum incubated without added particles, and the difference in hemolytic activity (ΔCCHA) between these samples was calculated according to Equations 2 and 3.

In serum from this Donor 1, the particles with a diameter of 250 nm potently activated the complement system, whereas the 50 nm or 600 nm particles showed substantially less activation when normalized to the total surface area of the particles (Fig. 1*A*). The activation clearly depended on either the classical or MBL pathways, as removal of Ca^{2+} ions essentially abolished complement activation (Fig. 1*B*). As expected, the addition of EDTA to the experiments abolished complement activation (data not shown). Zymosan, a particulate cell wall material from yeast, was included as positive control (Fig. 1*A*, 1*B*). To use the zymosan in a form comparable to the nanoparticles, we determined the diameter of the zymosan particles by DLS to be ~3000 nm (data not shown). The concentration of particles in suspension was determined by light microscopy, allowing for a comparison of the zymosan microparticles with nanoparticles based on total surface area applied to the experiments. The role of surface charge was investigated by application of iron oxide nanoparticles coated with carboxylated dextran; this modification of the dextran layer did not significantly change the complement activation (data not shown).

To investigate the variation among donors, the ability of the 50, 250, and 600 nm particles to activate complement in an additional seven sera were tested together with serum from Donor 1 (Fig. 1*C*); each particle type was added at a concentration corresponding to $A_{Tot} = 5 \times 10^{14}$ nm^2. The findings for Donor 1 were similar to experiments shown in Fig. 1*A* (i.e., with the strongest complement activation clearly induced by the 250 nm particles compared with the 50 nm and 600 nm particles). Compared to the data in Fig. 1*A*, however, differences in the absolute levels of hemolysis were noticeable. Although the results for donor sera shown in Fig. 1*C* were all generated with the same batch of rabbit Es to maximize comparability, this batch differed from that used for the measurements shown in Fig. 1*A*. It is an observation often made with hemolytic assays that ill-defined properties of the Es affect the level of complement-induced lysis (19). However, as shown by the comparison between Fig. 1*A* and 1*C*, this phenomenon did not alter the outcome concerning the strong complement activation by 250-nm particles compared with 50 nm and 600 nm in serum from Donor 1. The comparison among Donors 1–8 showed striking differences between the donors, both with regard to the interdonor variation in the level of complement activation as well as the

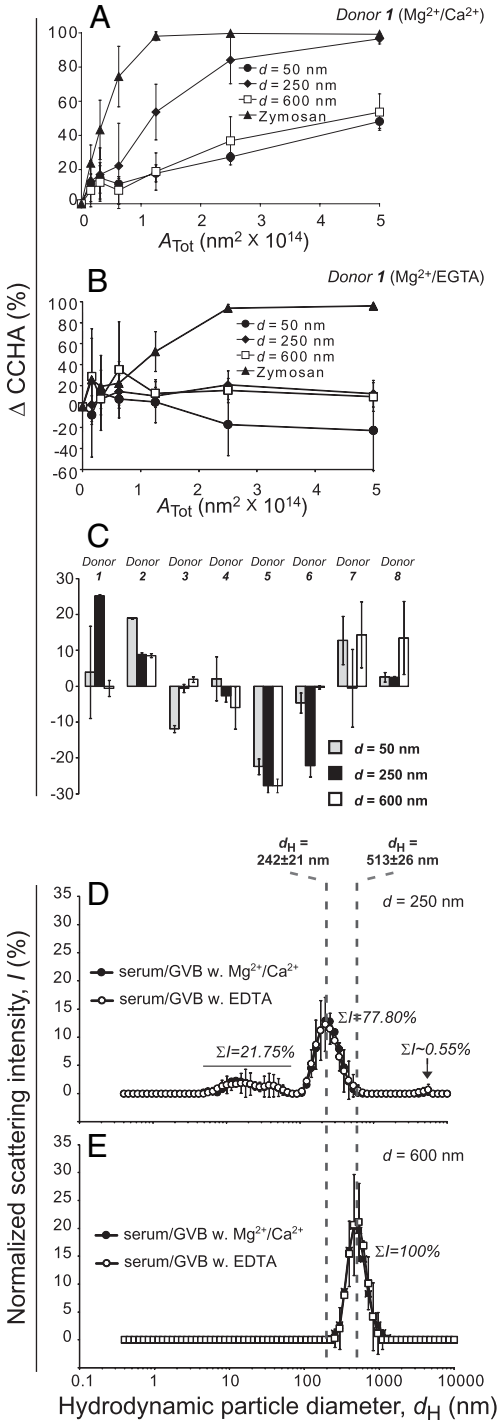

FIGURE 1. Complement activation by dextran-coated ironoxide nanoparticles. Nanoparticles, made from iron oxide and dextran, were tested for their ability to activate complement in serum from Donor 1. Comparison of the ability to activate complement by the differently sized particles was made according to total surface area (in nm^2) of particles added to the reactions. Following incubation of the particles in serum, either under conditions allowing for the activation through all complement pathways in the presence of Mg^{2+} and Ca^{2+} ions (*A*) or under conditions favoring activation through the alternative pathway in the presence of Mg^{2+} and EGTA (*B*), the percentage of CCHA was calculated according to Equations 3 and 4. In *A* and *B*, error bars show the SD on the mean value for 3–5 experiments. *C*, Variation among donors of the complement activation induced by nanoparticles investigated by the ΔCCHA assay. ΔCCHA was tested by incubation of serum with dextran-coated iron oxide nanoparticles with diameters of 50 nm, 250 nm, or 600 nm; each type of particle was tested with sera from 8 donors. Colloidal stability of nanoparticles in the presence of serum. Serum from Donor 1 diluted in either buffer with Mg^{2+}/Ca^{2+} (allowing for complement activation) or EDTA (blocking complement activation) was incubated with 250-nm (*D*) or 600-nm (*E*) iron oxide particles. The hydrodynamic particle diameters (d_H) in the serum suspensions were estimated by DLS and represented as the normalized scattering intensity (*I*) as a function of d_H with the sum of all intensities determined in the range of d_H from 0.4–10,000 nm equaling 100%. The contribution to the scattering of subsets of particles is indicated with Σ*I* followed by the percentage of the total scattering.

influence of particle type (i.e., particle diameter) on the complement activation.

A commonly observed phenomenon with nanoparticles in media containing serum proteins is aggregation. We investigated the role of complement in this process by comparing particles in serum either under conditions permitting complement activation (in the presence of Mg^{2+}/Ca^{2+}) or under conditions with no complement activation (in the presence of EDTA) but with exposure to the macromolecular constituents in serum (Fig. 1*D*, 1*E*). DLS measurements were performed on 250-nm and 600-nm iron oxide nanoparticles under the conditions used for the experiments shown in Fig. 1*A*. The light scattering by these particles was easily distinguishable from the contribution by serum proteins, the latter source contributing ~22% of the scattering intensity. The measured hydrodynamic diameters at 242 nm and 513 nm, respectively, were in acceptable agreement with the expected size, and the highly symmetric distribution of particle sizes suggested that the particles were essentially monodisperse. In the case of the 250-nm particles, a small contribution to the scattering intensity (0.55%) was observed for particles with d_H ~4000 nm (Fig. 1*D*). However, the scattering intensity of a particle is proportional to the diameter to the sixth power, whereas the volume is proportional only to the diameter to the third power (22). The difference implies that the volume of particles contributing this scattering constitutes <0.0002% of the volume of the 250-nm particles. Interestingly, the particle sizes did not differ between the conditions supporting complement activation (i.e., in the presence of Mg^{2+} and Ca^{2+} ions) and the conditions blocking complement activation (i.e., in the presence of EDTA) (Fig. 1*D*, 1*E*).

Donor variation in complement activation by nanoparticles investigated by C3a-des Arg measurements

As suggested by the analysis of serum from Donors 1–8, surfaces of particles with different diameter and hence curvature showed marked donor-dependent differences in their ability to activate complement (Fig. 1*A–C*). To investigate the role of particle size in complement activation further, we probed complement activation by the eight sera with the dextran-coated iron oxide particles by testing the generation of C3a-des Arg (32). The particle-induced complement activation was determined by subtraction of the concentration of C3a-des Arg in a sample of donor serum without added particles from the C3a-des Arg concentration in a sample with particles; the difference between these concentrations (ΔC3a-des Arg) measures the contribution of the particles to complement activation (Fig. 2*A*). In serum from Donor 1, the 250-nm particles released 24 μg (~3 nmol) of C3a-des Arg corresponding to the activation of $\sim 10^{15}$ C3 molecules when incubated in a total volume of 600 μl of serum-containing buffer. The total C3 concentration in serum from this donor was 7.7 μM (1.4 mg/ml), and hence the total number of C3 molecules in the reaction buffer was also $\sim 10^{15}$, suggesting that in the assay, ~100% of all C3 molecules were activated.

A common trait for six (Donors 1, 3, 5, 6, 7, and 8) of the eight donors was the poor complement activation by the 600-nm particles. Donor 6 showed a similar size preference as Donor 1,

whereas Donors 2 and 4 activated relatively indiscriminately on all three types of particles, including the 600-nm particles. Donors 5 and 8 showed no detectable complement activation by the nanoparticles compared with samples without particles. In the case of Donor 8, this finding was confirmed with additional analysis by the hemolytic assay described above (data not shown). A more rigorous analysis of these results was made by comparing the average complement activation for all donors with each type of particle (Fig. 2*B*). The median values also reflected the strong complement activation by the 250-nm particles, whereas the 600-nm particles were significantly less potent ($p < 0.01$).The complement activation by the 50-nm particles was highly variable among the donors, as reflected by the coefficient of variation (CV) (i.e., the SD for the ΔC3a-des Arg levels normalized by the mean value at 1931% compared with the values of 402% and 145% for the 250-nm and 600-nm particles, respectively).

Analysis of serum from Donor 1 showed that the alternative pathway did not contribute significantly to the complement activation on the dextran-coated particle surfaces (Fig. 1*B*). MBL deficiency is a common primary immunodeficiency in the complement system, and three of the tested sera were MBL-deficient (Donors 5, 6, and 7). However, reconstitution of MBL-deficient sera (Donors 5 and 8) with recombinant human MBL (33) had no influence on their ability to activate complement when mixed with the particles (data not shown). From these comparisons, we concluded that the classical pathway through binding of Abs to dextran on the particle surfaces was the major route of complement activation. To identify the antigenic structure recognized by these Abs, we also tested the ability of dextran-coated polystyrene particles to activate complement in serum from Donor 1 (Fig. 2*C*, 2*D*). Prior to the experiment, the polystyrene particles with diameters from 50 nm to 800 nm were incubated with dextran in solution. The low-m.w. dextran applied in these experiments was not capable itself of complement activation (data not shown). Suspensions with dextran and 100-nm polystyrene particles activated complement at levels comparable with the dextran-coated ironoxide particles (Fig. 2*A*, 2*C*). By contrast, the 50-nm particles as well as the particles with a diameter >100 nm failed to activate complement (Fig. 2*C*). None of the particles were capable of activating the complement system in the absence of dextran (Fig. 2*D*).

Donor variation in IgG and IgM dextran-binding activities

As shown above, the complement activation on the dextran-coated particles differed considerably between the donors (Fig. 2*A*, 2*B*); we investigated the variation in the binding activity of Abs to dextran. The TRIFMA signals for either IgG (Fig. 3*A*) or IgM (Fig. 3*B*) were plotted as a function of the serum concentration used in the wells. The binding activities observed using the sera from Donors 2–8 was estimated in units relative to the activity in serum from Donor 1 (Fig. 3*C*). The binding activity of IgM Abs in the eight sera exhibited a 250-fold difference between the highest and lowest binding activity found (Fig. 3*C*). In a similar comparison, the binding activities exhibited by IgG Abs showed a 17-fold difference (Fig. 3*C*). This finding was also reflected in calculations of the CV for the binding activities; the variation in IgM binding activities among the eight donors was almost twice as large as the variation in IgG activity (Fig. 3*C*).

Correlation between IgM binding activity to dextran and complement activation on the iron oxide particles

The relationship between the determined Ab-binding activities to dextran and actual binding of Abs to the dextran-coated particle surfaces was investigated by use of a modified TRIFMA. The 250-nm and 600-nm iron oxide particles were easily collected from the liquid suspension by either magnetic or centrifugal force, respectively, and

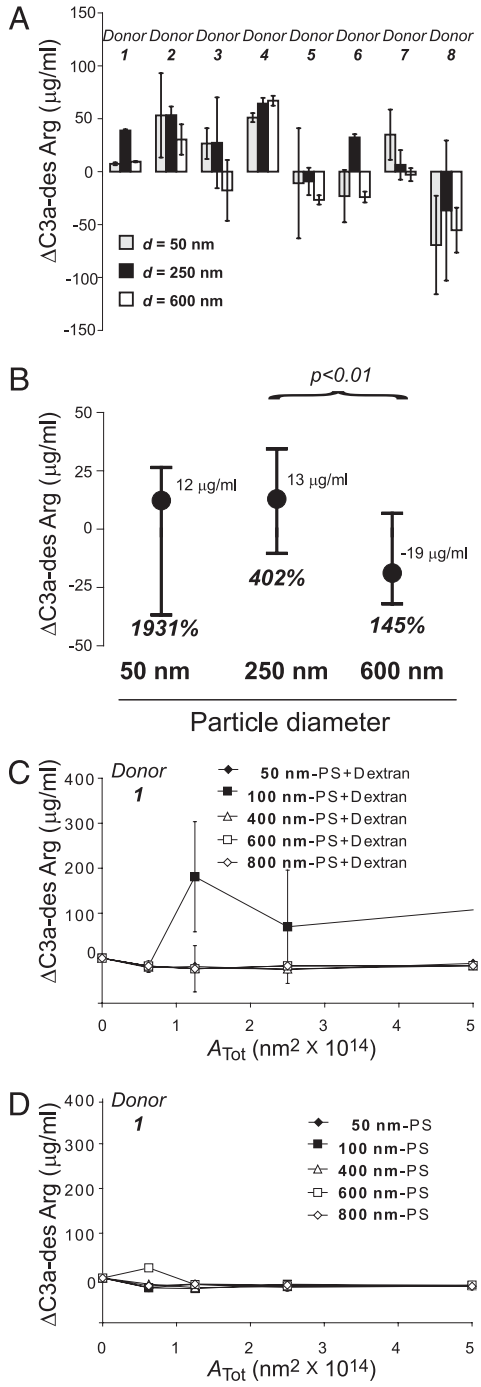

FIGURE 2. Variation among donors in the complement activation induced by nanoparticles tested by the generation C3a-des Arg. *A*, Release of C3a-des Arg from intact C3 through complement activation by dextran-coated iron oxide nanoparticles with diameters of 50 nm, 250 nm, or 600 nm; each type of particle was tested with sera from the eight donors also tested with the CCHA assay as shown in Fig. 1*C*. *B*, Statistical comparison of the complement activation on the iron oxide particles. The median value (indicated with a closed circle and in μg/ml) and CV (indicated in % in boldface and italic) were calculated for the ΔC3a-des Arg levels from Donors 1–8 for each type of particle. The scatter of the data was calculated as the difference between the 25% and 75% percentile indicated with bars. Statistically significant differences were probed in a Kruskal-Wallis test with Dunn's correction for multiple comparisons. Complement activation by polystyrene nanoparticles in buffer with dextran (*C*) or, as control, in buffer without dextran (*D*). In *A*, *C*, and *D*, error bars show the SD on the mean value for two to three experiments in duplicate.

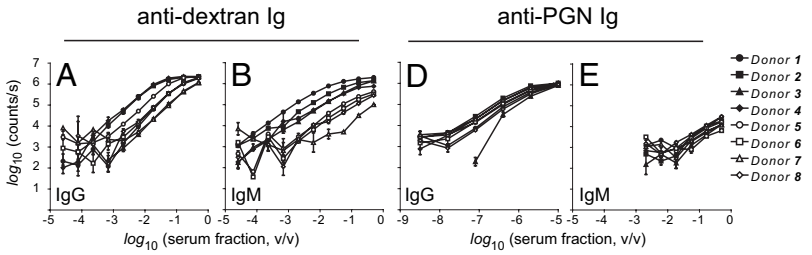

C

	anti-dextran IgG (mU/ml)	anti-dextran IgM (mU/ml)
Donor 1	≡1000	≡1000
Donor 2	7528 ± 1606	360 ± 33
Donor 3	543 ± 99	152 ± 8
Donor 4	9124 ± 1601	168 ± 20
Donor 5	3509 ± 59	32 ± 3
Donor 6	1096 ± 88	21 ± 1
Donor 7	515 ± 10	4 ± 1
Donor 8	1361 ± 139	15 ± 2
Mean (mU/ml)	**1858**	**201**
CV	**104%**	**170%**

F

	anti-PGN IgG (mU/ml)	anti-PGN IgM (mU/ml)
Donor 1	≡1000	≡1000
Donor 2	2898.1 ± 354.9	938.6 ± 84.7
Donor 3	680.2 ± 104.9	465.2 ± 28.2
Donor 4	1902.5 ± 82.2	552.5 ± 71.7
Donor 5	1466.6 ± 183.2	752.9 ± 38.6
Donor 6	1428.5 ± 397.5	280.0 ± 36.9
Donor 7	1947.9 ± 103.6	582.8 ± 29.1
Donor 8	725.8 ± 43.0	1346.6 ± 68.8
Mean (mU/ml)	**1506**	**740**
CV	**49%**	**46%**

FIGURE 3. Binding activities in donor sera of Abs to dextran or PGN. *A–C*, Binding of IgG or IgM to surfaces coated with dextran. The amount of bound IgG (*A*) or bound IgM (*B*) was estimated for Donors 1–8 in TRIFMA with the signal (in counts/s) plotted as a function of the serum concentration used in the wells. For each plot, the mean value and error bars indicating the SD for four measurements are shown. *C*, Relative IgG and IgM dextran-binding activities. The serum from Donor 1 was used as reference for the IgG- and IgM-binding activity and defined to contain a binding activity of 1000 mU/ml for both Igs. By comparing serial dilutions of sera from Donors 1–8, the relative binding activity was determined and expressed as a mean value (in mU/ml) and SD based on four experiments. The mean and CV were calculated for the IgG- and IgM-binding activities for the eight donors. *D–F*, Ab binding to PGN. Sera from the eight donors were added in serial dilutions to polystyrene wells coated with PGN. The amount of bound IgG (*D*) or IgM (*E*) was estimated from the signal in TRIFMA (in counts/s). Error bars state the SD on two to three independent experiments measured in duplicate. *F*, The relative binding activity to PGN of IgG and IgM was determined as in *C* from the titration of the eight donor sera shown in *D* and *E*, respectively, expressed as a mean value and the SD. The mean and CVs were calculated for the IgG- and IgM-binding activities for the eight donors.

we then compared the binding of IgG and IgM Abs to the particles (Fig. 4*A*, 4*B*). Based on the measured binding activities (Fig. 3*C*), we selected the three sera from Donors 1, 2, and 8. For both IgG and IgM, Donor 2 had dextran-binding activities higher than the respective mean values for the eight donors. Donor 1 had IgM-binding activity higher than the mean value for the donors, whereas the IgG-binding activity was lower than the mean value. For both IgG and IgM, Donor 8 had binding activities lower than the mean values. Consistently, the amount of bound IgG and IgM to the particle surface was clearly lower, and at the level of signal produced by a control Ab, when the particles were incubated with serum from Donor 8 compared with the signals obtained from incubation with sera from Donors 1 and 2 (Fig. 4*A*, 4*B*). The amount of bound Ig from incubations with these donors differed strikingly with regard to the signal for IgG, where the serum from Donor 2 produced a higher signal than the serum from Donor 1 consistent with the measured levels of IgG dextran-binding activity. Similarly, the near-equal ranking of the two sera with regard to the binding activity of IgM was confirmed by a quantitatively equal signal for the IgM binding to the particles for both 600-nm and 250-nm particles (Fig. 4*A*, 4*B*).

A central observation in this study was the ability of serum from Donor 1 to activate complement strongly on the surface of 250-nm particles but only weakly on the surface of the 600-nm particles (Figs. 1*A*, 1*C*, 2*A*). Nevertheless, the analysis presented in Fig. 4 showed that IgM bound equally well to the 600-nm (Fig. 4*A*) and 250-nm particles (Fig. 4*B*), implying that the surface densities of IgM on these particles were very similar. This finding suggested a preference of IgM for complement activation on the 250-nm particles compared with the 600-nm particles. We performed a more rigorous analysis of this hypothesis by comparing the generation of ΔC3a-des Arg (Fig. 2*A*) and the ΔCCHA (Fig. 1*C*) and IgM-binding activities (Fig. 3*C*) for the eight donor sera (Fig. 4*C*, 4*D*). In a nonparametric test (Spearman's rank-order correlation), the IgM-binding activities correlated significantly with complement activation measured by the ΔC3a-des Arg generation (Fig. 4*C*, 4*E*) for the 250-nm particles ($R = 0.74$, $p < 0.046$). As a control, we also investigated the correlation between the IgM-binding activities and complement activation on 600-nm particles, but, as expected from the findings mentioned above, no significant correlation was found for either the 600-nm or the 50-nm beads (Fig. 4*E*). Analyses of the IgG-binding activities (Fig. 4*E*) and ΔC3a-des Arg generation showed only poor correlations (R = ~0.21–0.41) and none that were statistically significant ($p < 0.36$–0.62). The correlation tests were also applied to ΔCCHA levels (Fig. 4*D*, 4*F*) for the eight donors shown in Fig. 1*C*. Similar to the analyses with complement activation measured through ΔC3a-des Arg generation, the correlation between binding activity to dextran and ΔCCHA had the highest R score for the correlation between IgM-binding activity to dextran and ΔCCHA levels for the 250-nm particles (Fig. 4*D*, 4*F*). Other correlation coefficients were at strikingly lower levels (R = ~0.00–0.45), although all correlations were nonsignificant (Fig. 4*F*).

Size-dependent complement activation by PGN

To inquire into the biological role of our findings above, we investigated the complement activation on bacterial surfaces using as a target PGN from *S. aureus*. Several investigations have already shown that *S. aureus* PGN is potent activator of complement, and, similar to the nanoparticulate system, our hypothesis was that primarily the size and hence topological features of the PGN fragments would contribute to the complement activation. Enzymatic digestion of purified PGN with lysostaphin, an endopeptidase that cleaves the PGN peptide bridges, and the muramidase mutanolysin, which cleaves the β-*N*-acetylmuramyl-(1→4)-*N*-acetylglucosamine linkage in the carbohydrate part of PGN, generated PGN fragments in a size range comparable to the

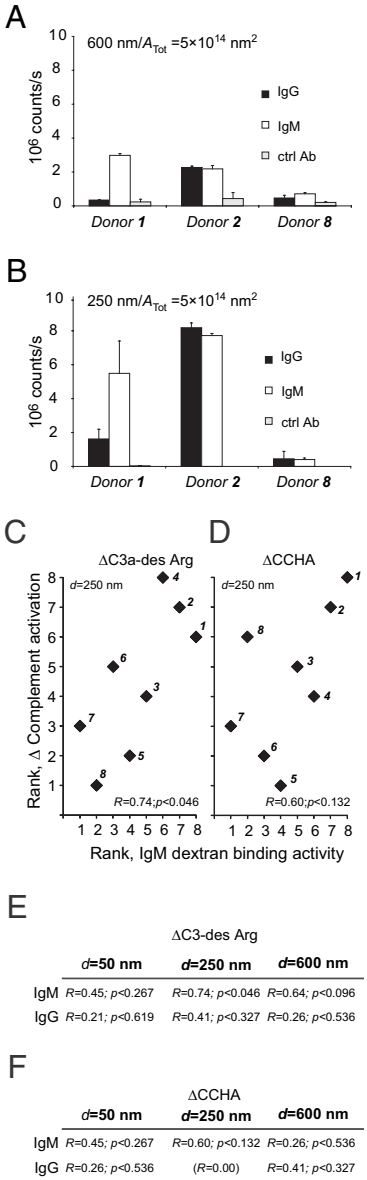

E

ΔC3-des Arg

	d=50 nm	*d*=250 nm	*d*=600 nm
IgM	*R*=0.45; *p*<0.267	*R*=0.74; *p*<0.046	*R*=0.64; *p*<0.096
IgG	*R*=0.21; *p*<0.619	*R*=0.41; *p*<0.327	*R*=0.26; *p*<0.536

F

ΔCCHA

	d=50 nm	*d*=250 nm	*d*=600 nm
IgM	*R*=0.45; *p*<0.267	*R*=0.60; *p*<0.132	*R*=0.26; *p*<0.536
IgG	*R*=0.26; *p*<0.536	(*R*=0.00)	*R*=0.41; *p*<0.327

FIGURE 4. Correlation between complement activation induced by the nanoparticles and binding activities of IgG and IgM to dextran. Serum from Donors 1, 2, or 8 was incubated with dextran-coated iron oxide particles with a diameter of 600 nm (*A*) or 250 nm (*B*). The binding of IgM and IgG to the nanoparticles was measured by TRIFMA with bars showing the mean value and error bars the SD for values from two independent measurements. Open bars show the binding of IgG, black bars the binding of IgM, and gray bars the binding of a biotinylated isotypic control Ab to the beads. *C* and *D*, The correlation between the IgM-binding activtity to dextran and complement activation induced by the 250-nm ironoxide particles was investigated by Spearman's rank-order test. *C*, For each donor (indicated with numbers 1–8 in the panel), the rank in complement activation measured by the ΔC3a-des Arg assay (as shown in Fig. 2*A*) was plotted against the rank in IgM-binding activity measured (as shown in Fig. 3*B*, 3*C*). The correlation coefficient (Spearman's *R*) and the level of significance (*p*) are indicated. *D*, The rank in complement activation measured by the ΔCCHA assay (as shown in Fig. 1*C*) was plotted against the rank in IgM-binding activity measured (as shown in Fig. 3*B*, 3*C*). As in *C*, the donors are indicated with numbers 1–8 together with the correlation coefficient and the level of significance. *E* and *F*, Coefficients and levels of significance for the correlation between complement activation by the 50-nm, 250-nm, or 600-nm particles measured by ΔC3a-des Arg assay and the IgM- or IgG-binding activities in the 8 sera (*E*). Similar analyses as in *E* were made based on the complement activation measured by the ΔCCHA assay.

nanoparticles employed earlier. Quantification of the size distribution in native PGN or following the enzymatic digestion was carried out with DLS (Fig. 5*A*). Untreated PGN presented a narrow size distribution of particles with a mean diameter of ~400 nm. Treatment with lysostaphin produced a number of particulate species with a diameter of 100 nm; a less well-defined peak around 500 nm probably reflected the presence of undigested PGN species in the reaction mixture. Double digestion of PGN with mutalysin and lysostaphin produced particles with a diameter of ~50 nm (i.e., significantly smaller than the particles found in untreated PGN as well as PGN digested with lysostaphin only). The double-digested PGN also provided a particulate material comparable to undigested PGN in size, whereas species with diameters of ~100 nm were not found.

The complement activation induced by PGN was measured as the generation of C3a-des Arg (32) compared with a control with no added PGN; the difference between these samples represented complement activation by the PGN preparations (Fig. 5*B*, 5*C*). In serum from Donor 1, PGN treated with lysostaphin induced a strong activation, whereas, by contrast, activation by either untreated PGN or doubled-digested PGN essentially failed to activate complement (Fig. 5*B*). The enzymes added to the PGN did not contribute to this activation. To analyze the pathway of complement activation, we measured the C3a-des Arg generation in samples without free Ca^{2+}, which reduced the complement activation by the lysostaphin-digested PGN. No C3a-des Arg generation was detectable in either of two C1q-deficient sera, which identified the classical pathway as the major contributor to the complement activation by the lysostaphin-digested PGN (Fig. 5*B* and data not shown).

We determined the relative concentrations of IgG and IgM Abs to PGN in the eight donor sera studied previously. *S. aureus* expresses Protein A, which binds strongly to human and mouse IgG; in the absence of serum application to the wells, only a minor signal (~2% of the signal intensity for wells incubated with serum used at the lowest dilution) was produced. This excludes Protein A contamination in the PGN preparation as a potential confounding factor in the assay. Using an isotypic control Ab rather than Abs to IgG or IgM gave similar low signals and confirmed the specificity of the assay. The TRIFMA signal from wells developed for either IgG (Fig. 3*D*) or IgM (Fig. 3*E*) were plotted as a function of the serum concentration used in the wells, and the binding activities were determined as for the binding activities to dextran (Fig. 3*F*). Among the donors, the variation in IgG- and IgM-binding activities to PGN was considerably smaller than the variation in the binding activities to dextran; compared with the CV values for IgG and IgM binding activities to dextran at 104% and 170%, respectively, the same CV values for the binding activities to PGN were 2–4-fold lower at ~50%. With regard to complement activation by these sera, the most striking finding was that undigested PGN activated complement very poorly, whereas PGN digested with lysostaphin induced a 2–10-fold stronger complement activation compared with untreated PGN (Fig. 5*B*, 5*C*). This was clearly reflected in a statistical comparison of the complement activation by the donor sera, where there was highly significant difference ($p < 0.001$) between the C3a-des Arg generation by PGN and PGN treated with lysostaphin (Fig. 5*D*). Two of the tested donor sera (Donors 1 and 6) showed a marked reduction in complement activation when the PGN was double-treated with both the lysostaphin and the mutanolysin compared with treatment with lysostaphin only, whereas sera from Donors 2 and 4 showed no difference in this comparison (Fig. 5*B*, 5*C*). Nevertheless, in a statistical comparison of levels of C3a-des Arg generation by the four sera, a significant reduction was found when PGN was treated

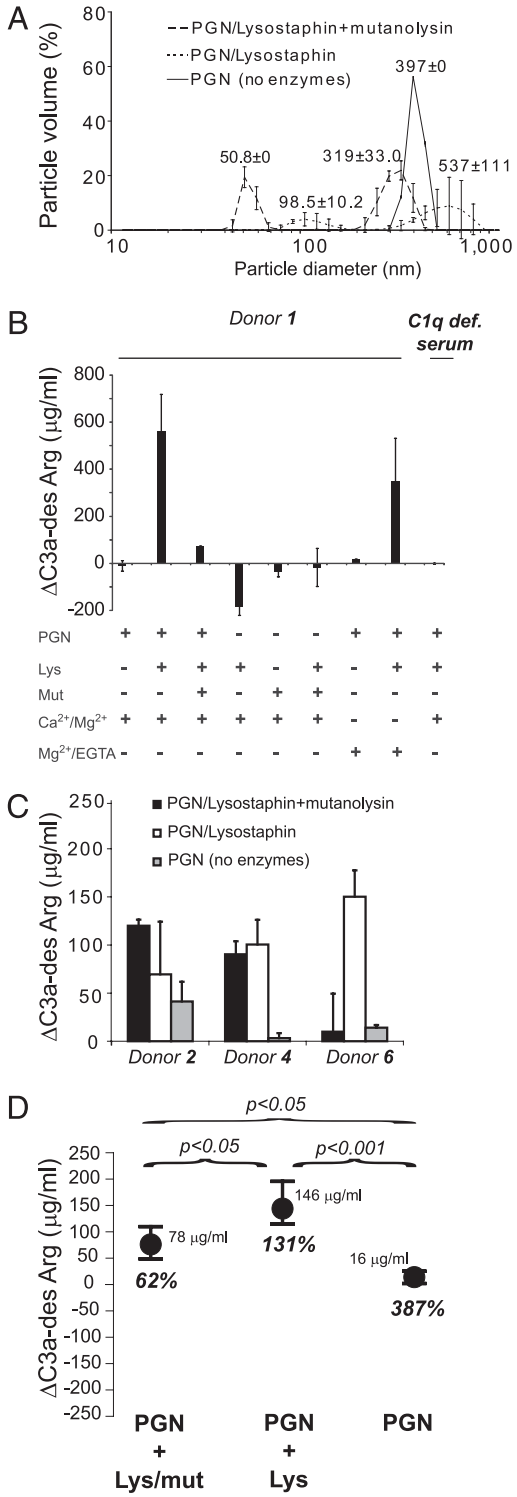

FIGURE 5. Complement activation (ΔC3a-des Arg) by intact and fragmented PGN from *S. aureus*. *A*, The relative size distribution of particulate PGN (expressed as a percentage of total particle volume) for native PGN (solid line), following fragmentation by digestion with lysostaphin (dotted line), or following digestion with lysostaphin and mutanolysin (hatched line). For each curve, peaks in particle volume are labeled with the corresponding particle diameter. *B*, Analysis of the influence of enzymatic digestion on the complement activation by PGN in serum from Donor 1. The contribution by the complement activation pathways was analyzed by modifying the presence of divalent cations or conducting the experiment in C1q deficient serum. *C* and *D*, Comparison between donors of PGN-mediated complement activation. *C* shows the complement activation by PGN and digested PGN in sera from Donors 2, 4, and 6. For each source of PGN, each bar shows the mean value and the error bars the SD from two experiments in duplicate. In *D*, the median value (indicated with a closed circle and in μg/ml) and CV (indicated in % in boldface and italic) were calculated for the ΔC3a-des Arg levels from Donors 1, 2, 4, and 6 for each type of particle. The scatter of the data was calculated as the difference between the 25% and 75% percentile indicated with bars. Statistically significant differences between the complement activation by PGN preparations were probed in a Kruskal-Wallis test with Dunn's correction for multiple comparisons.

with lysostaphin and mutanolysin compared with treatment with lysostaphin only (Fig. 5*D*).

Bacterial growth liberates complement-activating cell wall fragments

Our findings above prompted us to investigate whether the normal physiology of *S. aureus* involves the generation of fragments of the cell wall. To probe the chemical nature and ultrastructural properties of the particulate material generated during bacterial growth, we cultured the *S. aureus* and analyzed the cells and supernatants by AFM and TEM.

AFM provides topographical information on the ultrastructure of the applied specimen. Clusters of *S. aureus* cells (Fig. 6*A*, 6*C*) were investigated by analyzing height profiles as shown in Fig. 6*B*, 6D through sections indicated in the AFM images with bars (Fig. 6*A*, 6*C*). The profiles showed curvatures with estimated diameters close to the diameters of single cells. However, structural features with less rounded profiles and dimensions significantly smaller than single cells were also visible; the approximate cross-sectional diameter of these fragments appeared over a range of 158–367 nm estimated as shown in Fig. 6*B* and 6D. These fragments apparently had a considerable sharper curvature than the intact bacteria.

We wished to analyze whether the *S. aureus* fragments identified by AFM were liberated into solution during culture of the bacteria. With this aim, we filtered the bacterial culture through a 0.22-μm filter to remove intact cells, embedded the samples in agarose, and analyzed by TEM 60-nm-thick sections (Fig. 6*E–G*). Untreated filtrate (Fig. 6*E*) contained species with a width of ~20 nm and reminiscent of fibrous material. The fragments had lengths of 100–300 nm, but fragments larger than this were also present. The composition of the fragments was analyzed by treatment with two endopeptidases specific for either PGN or proteins. Treatment of the filtrate with lysostaphin gave a blurred or diffuse outline and a slight increase in the width of the fragments (Fig. 6*F*). This appearance was not a consequence of the imaging of these specimens because altering the focus plane or a change in contrast or brightness of the TEM image could not restore the sharp outline of the untreated PGN (Fig. 6*E*). For comparison, we also treated the filtrate with the serine protease trypsin that promiscuously digests proteins. The peptide bridges in PGN are not substrates for trypsin, which usually cleaves on the C-terminal side of positively charged residues. Compared with the untreated sample (Fig. 6*E*), the treatment with trypsin only produced a minor change in the appearance of the fragments, which, in general, preserved their contrast and length (Fig. 6*G*).

Many of the PGN fragments identified by TEM in the culture medium showed a homogeneous curvature unlikely to originate from random folding in the medium (Fig. 6*E*) and similar to curved PGN fragments that have been reported in other studies (12, 34). To obtain a robust quantification of the curvature of these fragments, we applied a comprehensive analysis to extract an estimation of the curvatures from all the visualized fragments. As shown in Fig. 7*A*,

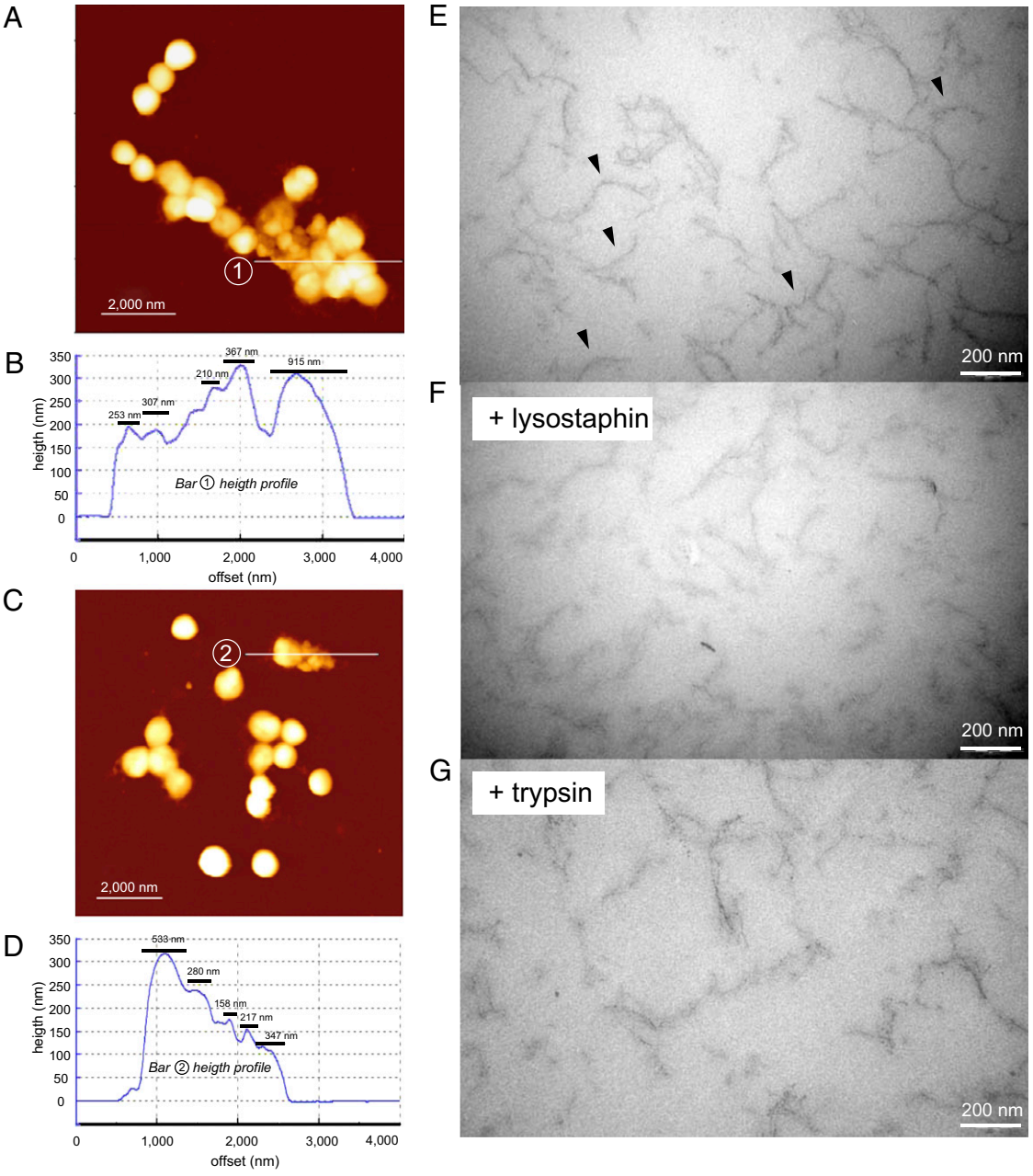

FIGURE 6. Analysis of bacterial fragmentation during culture. *A–D*, Samples of fixed *S. aureus* cells were analyzed by AFM. The cells were applied to glass slides and imaged in the dry state; two images are shown (*A* and *C*) with a scale bar indicating a path of 2000 nm in the plane of the image. The height contours of cell clusters were determined by following a trajectory of 4000 nm, as indicated with thin bars and a number; the profile matching bar 1 is indicated in *B*, and the profile matching bar 2 is indicated in *D*. For each profile in *B* and *C*, bars are added indicating the approximate span of individual structural features. *E–G*, TEM micrographs of a culture of *S. aureus* filtered through a membrane with a pore size of 0.22 μm to remove intact cells. Each micrograph is shown with a 45,000-fold magnification of the specimen. The culture medium was analyzed either in an untreated state (*E*) or following treatment with either lysostaphin (*F*) or trypsin (*G*). In *E*, arrowheads are placed to indicate examples of fragments with a curvature that probably results from tension in the PGN layers; similarly curved PGN fragments have been reported in other studies (12, 34)

the two-dimensional curvature at each pixel along the path of a fragment was estimated from the diameter of the largest circle fitting the path curvature at that position, and the curvature was calculated according to Equation 5. To bring the calculated curvatures onto a scale comparable to the size of the Abs binding to PGN, we calculated the mean curvature for segments with a length of 35 nm (i.e., the cross-sectional diameter of IgM). The distribution of these mean curvatures for the PGN fragments in the culture medium is indicated in Fig. 7*B*. Apparently, the most frequent curvature occurred at ~0.03 nm^{-1}. To aid the interpretation of this value, the two-dimensional curvatures according to Equation 5 of spherical objects with diameters of 50, 100, and 1000 nm are also indicated (Fig. 7*B*). This comparison showed that the mean curvatures of the PGN fragments came close to the curvature of a particle with a diameter of 100 nm. The curvature of a particle with a diameter of 1000 nm (i.e., close to the diameters of intact *S. aureus*) (Fig. 6*A–D*) was almost an order magnitude smaller than the more frequent curvatures of the PGN fragments.

The ultrastructural properties of the PGN fragments released from the cultured bacteria suggested that these fragments had curvatures that would facilitate complement activation through IgM binding as inferred from our studies of the dextran-coated iron

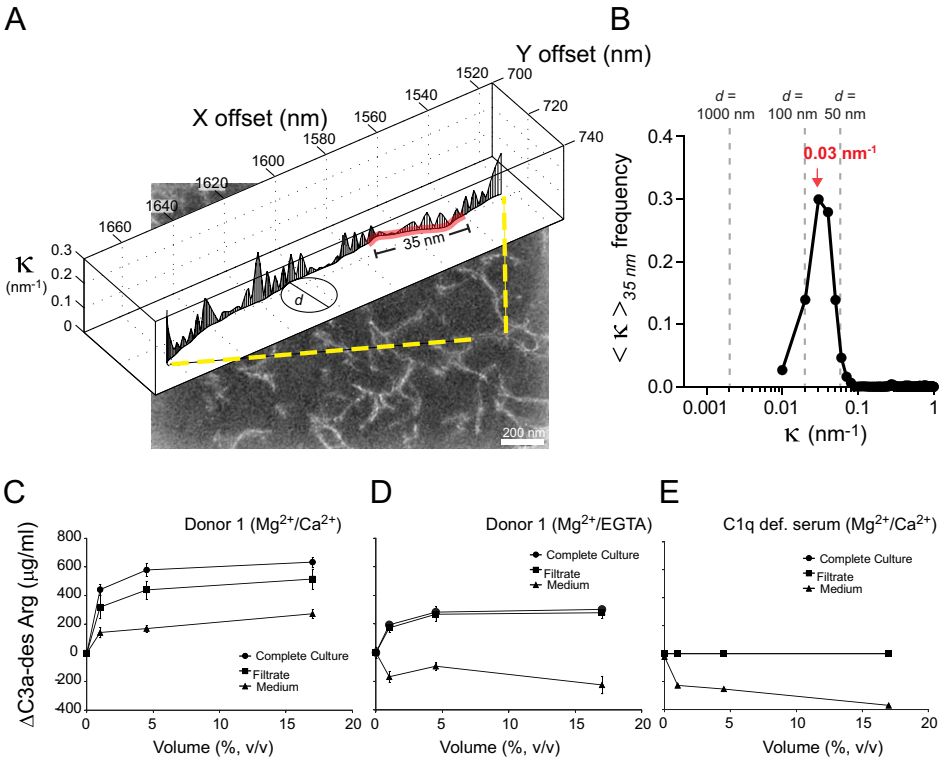

FIGURE 7. Curvature of *S. aureus* cell wall fragments and their ability to activate complement through the classical pathway. *A* and *B*, The curvature of cell wall fragments was assessed from the TEM micrograph shown in Fig. 6*E*. For each pixel in the fragments, κ was calculated from Equation 5 as described in *Materials and Methods*. Mean curvatures ($<\kappa>_{35\ nm}$) along segments of 35 nm (i.e., the cross-sectional diameter of IgM) were calculated for all fragments shown in the TEM micrograph. In *B*, the frequencies of $<\kappa>_{35\ nm}$ were plotted as a function of κ. For comparison, the curvatures of spherical particles with diameters of 1000 nm, 100 nm, and 50 nm are indicated. These values match the diameters of intact *S. aureus*, fragments of PGN digested with lysostaphin, and fragments of PGN digested with lysostaphin and mutanolysin, respectively. *C–E*, Complement activation by complete bacterial cultures or culture filtrate without intact bacteria. Complement activation was measured by diluting complete overnight culture of *S. aureus* in serum followed by incubation under conditions allowing for complement activation through all pathways (*C*) or in the presence of Mg^{2+}/EGTA, thereby reducing the activity of classical pathway (*D*), or in the absence of C1q abolishing classical pathway activity (*E*). Comparisons were made between complete bacterial culture (i.e., growth media with bacteria), a filtrate of the complete bacterial culture (i.e., growth media with intact bacteria removed by filtration), or pure culture medium.

oxide particles as well as the enzymatically digested PGN. By contrast, *S. aureus* would mainly present PGN in an intact cell wall with a curvature that would be unlikely to support complement activation through conformational regulation of the surface-bound Abs. From these considerations, we hypothesized that the liberated PGN fragments would be relatively potent in complement activation compared with the intact bacteria and constitute the major source of complement-activating bacterial metabolites in an *S. aureus* culture. Medium containing the PGN fragments only was prepared as for the microscopic analysis by removing the intact bacteria through filtration. Complement activation by this source was compared with a culture of *S. aureus* containing both bacteria and fragments. As a reference, the complement activation by fresh medium was also analyzed (Fig. 7*C*). The presence of bacterial macromolecules enhanced complement activation compared with fresh medium as shown by the addition of either complete *S. aureus* culture or a filtrate of the culture. Our analysis also showed that removal of the intact bacteria by filtration did not significantly alter the potency of complement activation by the medium; this finding identified the bacterial macromolecules in the filtrate as the major source of complement activation in the complete culture. Similar to the investigations made earlier, the contributions by the complement activation pathways were studied by conducting the experiments in the absence of Ca^{2+} ions (Fig. 7*D*) or in serum deficient in C1q (Fig. 7*E*). Under these conditions, the complement activation was either reduced (Fig. 7*D*) or completely blocked (Fig. 7*E*), respectively, pointing to the classical pathway of complement activation as the major contributor to the complement activation.

Discussion

In this study, we show that simple binding of IgM to a surface with target Ags is not sufficient to activate the classical pathway of complement activation. For successful complement activation following IgM binding, a particular surface must satisfy specific topological criteria, especially regarding curvature.

The importance of curvature for complement activation was demonstrated using a chemically and structurally well-defined system of iron oxide or polystyrene particles with a dextran coating. Given that IgM is a strong complement activator with as little as one molecule bound to the surface of RBCs sufficient to mediate lysis (35), it is a quite surprising finding that the 600-nm particles on one hand bound IgM as effectively as the 250-nm particles but failed to induce complement activation, whereas on the other hand, only the 250-nm particles induced such activation. This difference in complement activation, measured as the particle-induced generation of C3a-des Arg, was further confirmed by a study of sera from a total of eight donors. The median level of ΔC3a-des Arg generated from incubations with the 250-nm particles exceeded significantly that obtained from incubations with the 600-nm particles. A more complex pattern of activation appeared to be the case for particles with a diameter of 50 nm. Sera from at least two donors failed to

activate complement on the 50-nm particles, whereas strong activation was found following incubation of the same sera with the 250-nm particles. This is supported by a recent proteomic study in which it was reported that 50-nm particles were poorly opsonized by complement (36). However, the median ΔC3a-des Arg level following incubations of the eight sera with 50-nm particles did not differ significantly from the level measured following incubations with the 250-nm particles. In terms of quantifying the deposition of C3 fragments on the particle surface, we compared the particle-induced release of C3a-des Arg with the total C3 concentration in serum from Donor 1 and found that 100% of C3 was activated during incubation with the 250-nm particles. Recent crystallographic analyses of the structure of C3b (37, 38) suggest that each surface-bound molecule covers an area on the particle of ~40 nm^2. If all activated C3 were attached to surfaces, the protein would cover a total area of 4×10^{16} nm^2, which is 80-fold larger than the supplied total surface area of the nanoparticles at 5×10^{14} nm^2. However, our studies with DLS found no significant increase in particle diameter, indicating that the great majority of activated C3 molecules are released into the surrounding medium rather than being deposited on the particles surface. This is consistent with the findings by other studies using radiolabeled C3 (39).

To compare the findings for Ab binding to the iron oxide particles with binding to a more natural target, we included a study on complement activation using cell wall material from the Gram-positive pathogen *S. aureus*. Through enzymatic digestion, we prepared samples of PGN-containing particles with hydrodynamic diameters of ~100 nm or ~50 nm. Compared to the untreated material with a hydrodynamic diameter of ~400 nm, the preparations containing smaller particles significantly enhanced the complement activation. Two of the four donors tested (Donors 1 and 6) showed profiles with the strongest complement activation by intermediate-sized PGN with a hydrodynamic diameter of ~100 nm, whereas the PGN with either smaller (~50 nm) or larger diameters (~400 nm) activated less strongly. This is in accordance with the results from incubations with dextran-coated iron oxide and polystyrene particles, where similar-sized particles produced the strongest complement activation. Furthermore, as shown by comparison with controls, the complement activation by both dextran-coated nanoparticles and PGN was dominated by the classical pathway, whereas neither the alternative pathway nor MBL apparently contributed to the activation.

Further details of the mechanisms responsible for complement activation by the dextran-coated nanoparticles and the digested PGN were provided from measuring the binding activities of IgG and IgM Abs to dextran and PGN in the donor sera. In particular, the IgM-binding activity to dextran showed a large variation between donors. In itself, this suggests that IgM Abs are responsible for the considerable donor variation observed. A more formal test of the role of IgM was carried out by correlation analyses, which showed that IgM dextran-binding activity correlated significantly with ΔC3a-des Arg for complement activation by the 250-nm, but not by the 50-nm or 600-nm, particles. These analyses did not identify a distinct role of IgG in complement activation by the dextran-coated nanoparticles. We also analyzed complement activation by the hemolytic assay and correlated the Ig-binding activities to the ΔCCHA levels. Similar to the analysis with ΔC3a-des Arg as a measure of complement activation, the highest correlation coefficient was found for the comparison of IgM dextran-binding activities and the complement activation by the 250-nm particles. However, this correlation was not statistically significant. It should be noted that ΔCCHA as a measure of complement activation in interdonor comparisons is a more complex parameter than ΔC3a-des Arg. Firstly, because the readout in the hemolytic assay depends not only on the activation of C3 but also on the donor-derived components of the lytic pathway (i.e., C5–C9), sources of variations not affecting the generation of C3a-des Arg may influence the hemolytic assay. Secondly, the higher complexity of the chemical processes leading to lysis of the Es obviously complicates the interpretation of differences found in ΔCCHA levels, notably in the correction for the non–particle-dependent complement activation in serum heated to 37°C. By contrast, the concentrations of C3a-des Arg maps onto a linear scale and hence the concentrations measured in serum samples incubated with nanoparticles are more easily compared with control experiments (i.e., by simple subtraction of the background activation).

Both previously published studies as well as ours (16) found that IgG and IgM Abs to PGN are frequent among donors with little variation in titers or binding activity. With the minor variation in IgG- and IgM-binding activities, we were not capable of separating the role of these isotypes in complement activation by the PGN samples through correlation analyses. However, a statistical analysis including the four sera showed a strong preference for activation on the lysostaphin-treated PGN and containing particles with a diameter of ~100 nm, consistent with the presence of IgM Abs to PGN in all donor sera. Earlier studies also reported that enzymatically treated PGN was a more potent activator of complement than untreated PGN, with the interpretation that the increase in activation was due to the enzymatic generation of neoepitopes (17). However, as demonstrated in our analysis, despite easily detectable binding activities of Abs to untreated PGN, the donor sera essentially failed to activate complement with this material; Ab binding per se is consequently not sufficient for complement activation. Treatment with two enzymes with distinct substrate specificities, which would be expected to enhance the generation of neoepitopes, quenched the complement activation, also arguing that altered epitope expression was not an explanation of why digestion of PGN promoted complement activation. By analogy with our observations on complement activation by the particles with defined curvatures, we suggest that the altered curvature of digested PGN is a critical parameter for the enhanced activation by enzyme-treated PGN; indeed, this suggestion is supported by our quantitative analysis of the size of the PGN fragments that activate complement.

Considerable efforts have been invested in characterizing the processes of *S. aureus* cell division that involves splitting of the cell wall. By contrast, little has been published on the ultrastructure of the byproducts of this activity, although from the current models of cell division, it seems clear that release of PGN fragments from the intact cells is a likely outcome (12, 34). The sizes of these fragments differ considerably, although the ability of the fragments, but not intact *S. aureus*, to pass through the 0.2-μm filter pores suggest that the fragments are significantly smaller than intact cells. Treatment with lysostaphin induced a diffuse staining pattern in the TEM micrographs that has been reported earlier for lysostaphin digestion of the cell wall of *S. aureus* (40) and confirms PGN as a major constituent of the fragments. Although DLS proved a convenient way of obtaining information on the size distribution of PGN fragments following the enzymatic digestion, the considerably more complex mixture of PGN fragments from the *S. aureus* culture could not be analyzed by this approach. We extracted information on the curvatures of these fragments from the TEM imaging. Our analysis showed that these fragments include curvatures comparable to particles with diameters of ~50–100 nm (i.e., much sharper than would be the case for the PGN layer in intact *S. aureus* cells, which have a diameter of ~1000 nm). Although some mathematical sophistication was required to arrive at this point, it seems intuitively to make sense from what is known about the properties of PGN; the PGN cell wall is an exoskeleton with internal tension forces that supports contouring of the cellular shape

(12, 41). In the event of liberation and fragmentation of the PGN cell wall, these forces may act to produce a sharper curvature of the PGN compared with the PGN in the intact cell wall.

The relationship between surface curvature and IgM-mediated complement activation raises an interesting question concerning the contribution to these processes by intact *S. aureus* versus their cell wall fragments. Unlike the common assumption that intact bacteria are the major targets of complement deposition, our findings suggest that the liberated PGN fragments could account for a significant part of the complement activation by a bacterial culture. By comparison of PGN and enzymatically digested PGN, we have already shown that the sp. act. of PGN fragments is higher than the undigested, and hence relatively intact, PGN layer. We chose to compare the complement activation by a complete *S. aureus* culture versus a sterile filtrate omitting the intact cells. We show that complement activation by the filtrate is almost as strong as that exhibited by the complete culture, clearly attributing much of the complement activation to bacterial products in suspension. As it is already known that PGN is the major source of complement activation among the metabolites of *S. aureus* (15), it seems reasonable to suggest that it was indeed the PGN fragments in the filtrate contributing to the activation of the complement system. In C1q-deficient serum, no complement activation was observed, supporting our suggestion that an Ab-dependent mechanism of complement activation is important for the relatively high activity of the PGN fragments compared with intact bacteria. Although we suggest that the curvature of the PGN fragments and the intact bacteria are one significant parameter in making the fragments relatively potent in complement activation, it is certainly possible that other factors such as the complex composition of the intact *S. aureus* cell wall (12) contributes to a lowering of the complement activation by the intact bacteria. However, this only strengthens the point that liberated PGN fragments are relatively potent activators of the complement system compared with intact bacteria.

A structural rationale for explaining the role of target surface curvature in IgM-mediated complement activation has already been proposed through the work of Perkins et al., Feinstein et al., and Feinstein and Munn (7, 9, 10). The diameter of the dextran-coated iron oxide and PGN particles probed in our study comes close to the cross-sectional diameter of the planar IgM molecule in solution at 35–38 nm, and the curvature of the surface is consequently significant compared with the IgM molecule (Fig. 8*A*, 8*B*). This is also evidently the case for the conformation of IgM unmasking binding sites for C1q in the Cμ2 domains (i.e., the staple-like conformation with the Fabs bent at an angle (φ) of 60° relative to the Fc_5 disk including the J chain) (Fig. 8*B*). From a model of this conformation, we were able to obtain information of certain geometric properties of IgM. From a careful determination of the centroid of the Fc_5/J chain disk (Fig. 8*A*), the distance from the centroid to the hinge (the distance *SB* in Fig. 8*A–C*) was determined to be 8.58 nm, and from the hinge to particle surface (the distance *SR* in Fig. 8*B*, 8*C*), the distance is 10.67 nm. The geometric relationship between angles and distances for the particle-bound IgM is shown in a two-dimensional representation in Fig. 8*B*. The binding between the IgM Fab and the particle is characterized by the angle α between the tangent to the circle at point *R* and the line *SR* with the angular relationship $\theta = \varphi - \alpha$. From trigonomic considerations, it was possible to establish Equation 6 relating *SR*, *SB*, φ, α, and *CR*, which is the radius of the circle:

$$SR \cdot \cos\varphi + SB = CR \cdot \sin(\varphi - \alpha) \cdot \qquad (6)$$

For a constant value of φ, Equation 6 has a simple analytical solution (Fig. 8*D*). With $\kappa = 1/CR$, using Equation 5, it is possible to plot α as a function of curvature for φ at a constant value of 60° (Fig. 8*D*). The plot clearly shows that α changes as a function of the particle curvature when φ is kept at the 60° critical for complement activation. The binding interface between a paratope in the Fab fragment and the Fab-bound epitope on the surface would similarly change if the curvature of the surface were changed over the range matching our experimental work. Although certain epitopes could be speculated to comply with Fab binding over a range of values of α, it should be noted that usually the buried surface between paratope and epitope is large and consequently not likely to accommodate much variation in the binding interface (6). The role of the cell wall as an exoskeleton as well as the construction of the wall from repeating disaccharide-peptide units (12) suggest a certain molecular rigidity combined with a repeated and highly similar presentation of epitopes on the surface of such material. Consequently, the orientation of Fabs binding their cognate PGN epitope would be reasonably constant for epitopes exposed across the PGN layer, reflected in a more or less constant value of α for such interactions. Based on the assumption that the strong complement activation by the liberated PGN fragments (with a curvature of 0.03 nm^{-1}) reflects a prominent exposure of C1q binding sites upon IgM binding to these fragments (i.e., φ ~60°), it is possible from Equation 6 to estimate a value of α of 33°. Although there is no simple analytical solution to Equation 6 with φ as a variable, numerical solutions for φ with curvatures in the range of 0.002–0.05 nm^{-1} (corresponding to particle diameters in the interval 40–1120 nm) are shown in Fig. 8*D*. As indicated, φ takes a value of only 30° on surfaces with a curvature similar to spherical *S. aureus* cells ($d = 1000$ nm), whereas particles with curvatures in the range of 0.02–0.04 nm^{-1} (i.e., $d = 50$–100 nm) brings φ much closer to the conformational requirement for complement activation. All curvatures in this interval and with the chosen values for α support binding of the IgM molecule with distances from the centroid in the Fc_5/J chain disc to the particle surface (i.e., *BN* in Fig. 8*C*) vastly larger than 0 nm (Fig. 8*D*). This suggests that all conformations involved are structurally meaningful and qualitatively similar (i.e., variants of the staple-like conformation). Our findings are in quantitative agreement with findings from complement activation by enzymatically degraded PGN, where the fragments with a d_H of ~100 nm activated complement significantly better than intact PGN with a d_H of ~400 nm. An interesting perspective arises from considerations of the three-dimensional interaction between IgM and PGN. If indeed α is a constant, the 5-fold rotational pseudosymmetry of IgM also suggests that the epitopes must be organized in a pattern with rotational symmetry for supporting binding by all Fabs. Examination of the structure of PGN on the bacterial cell surface with AFM and electron microscopy showed that newly synthesized PGN is organized with an infrastructure of concentric rings with a spacing of 13–25 nm (42), implying that the IgM molecule can span at least some of these rings. This also suggests that the epitopes are organized in concentric rings, and liberated PGN with such structural properties would consequently easily form high-avidity interaction with IgM Abs.

Our model may also account for the observation that complement activation by the dextran-coated particles was highly variable for the 50-nm particles, whereas the 250-nm particles induced a more stable level of complement activation among the tested donor sera. The solution structure of IgM is planar and apparently stable in solution (7). Consequently, energy is required for deflection, or bending, of the IgM solution structure, which is likely to be contributed by the

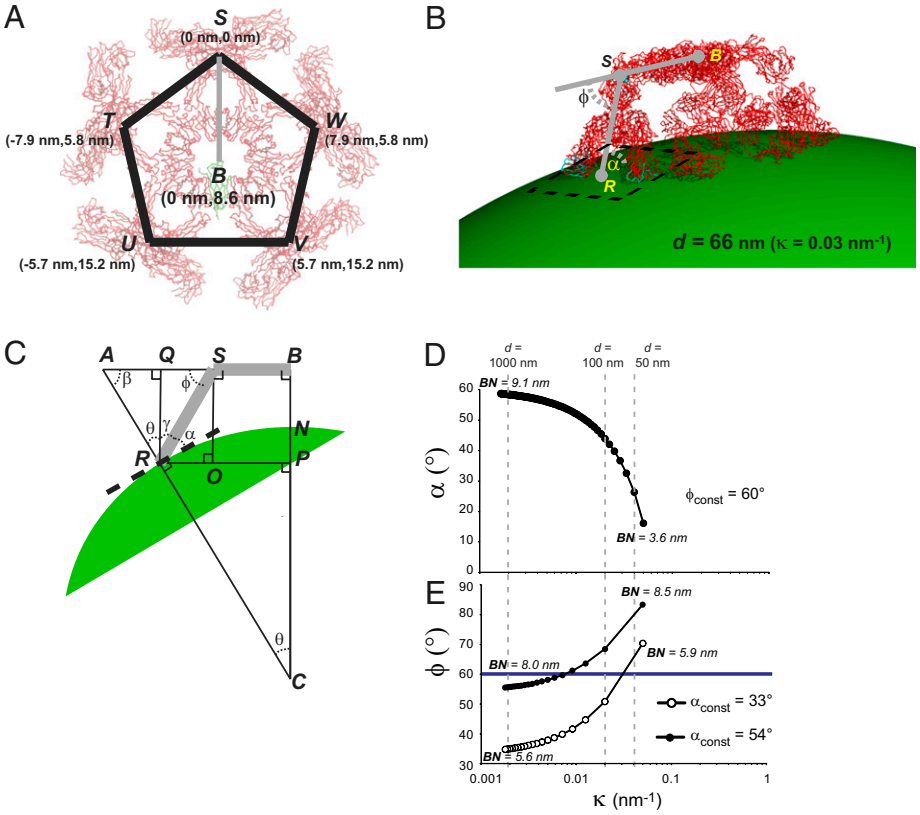

FIGURE 8. Model of the structural requirements for the binding of IgM in the staple-like conformation (8–10) to epitopes exposed on the surfaces of nanoparticles with differing curvatures. *A* and *B*, A pseudoatomic model of the IgM pentamer in the staple-like conformation was made from the planar solution structure of IgM reported by Perkins et al. (7) using the coordinates found in the Research Collaboratory for Structural Bioinformatics Protein Data Bank (www.pdb.org/) with the entry number 2RCJ. The regions corresponding to the five $F(ab')_2$ were rotated 60° downward with respect to Fc_5/J chain disc and molecular graphics images produced using the UCSF Chimera package (48). As shown in *A*, the centroid (*B*) of the Fc_5 disc, including the J chain indicated in green, was determined from considering the distances in two dimensions between equivalent residues (indicated with *S*, *T*, *U*, *V*, and *W*, respectively) located in the Cμ2 domains (i.e., the hinge between the Cμ1 domain and the Fc_5/J chain disc). From these calculations, the distance *SB* was 8.6 nm. In *B*, the IgM molecule in the staple-like conformation is shown on the surface of particle with a diameter of 66 nm (i.e., with a curvature) (κ = 0.03 nm^{-1}) corresponding to the PGN fragments analyzed in Fig. 7*A* and 7*B*; the variable loops are indicated in blue. The point *R* on the particle surface was placed equidistant between the variable loops of a $F(ab')_2$ on a line through the Cμ1 domains as indicated in the figure. The distance *SR* equals 10.6 nm. *C*, Two-dimensional representation of geometric relationship between angles and intramolecular distances of the IgM molecule (sketched in gray). The angle φ measures bending of the Cμ1 and variable domains relative to the Fc_5 disk, whereas α measures the angle between the line *SR* and the tangent to the circle with a radius *CR* (i.e., the particle surface) at the point *R*. *D* and *E*, Relationship between the angles α, φ, and the curvature of the particle κ. With φ at a fixed angle (60°), there is an analytical solution of the following equation for α as a function of: κ: $\alpha = \arcsin([SR \cdot \cos\varphi_{const} + SB]/CR) - \varphi_{const}$. Based on this function, α was plotted as a function of κ in *D*. In *E*, values of φ were plotted as a function of κ with α at a fixed value of either 33° or 54°. Equation 6 was solved numerically using an HP48SX calculator (Hewlett-Packard, Palo Alto, CA). For each plot in *D* and *E*, the shortest distance from centroid in the Fc_5/J chain disc to the particle surface (the distance *BN* in *C*) is indicated for the minimum and maximum values of κ.

energetically favorable interaction between paratope and epitope. For high-affinity interactions, it is probably possible to strain the IgM molecule more than would be possible for weaker interactions. Based on calculations similar to those made for PGN, we estimated from the high complement activation on 250-nm particles that α on the dextran surfaces takes a value of ~54° (Fig. 8*E*). However, this is likely to represent an overestimate, as we also found strong complement activation on dextran-coated 100-nm polystyrene particles as well as in some cases on the 50-nm dextran-coated iron oxide particles. As shown in Fig. 8*E*, it is clear that the degree of straining (φ) grows rapidly for particles with diameters of the order of 50 nm. We suggest that the variability found in our assays reflects variations in the affinity of IgM Abs to dextran with only some donor sera presenting Abs with sufficiently high affinity for accommodating binding to the 50-nm particles.

Unlike Gram-negative bacteria where 60% of the PGN is recycled (43), Gram-positive bacteria release PGN as shown in our and several other studies (13, 44). Although several routes for PGN-mediated stimulation of the immune system have been identified, it nevertheless remains unclear whether the released PGN play specific roles in the pathophysiology of infections with Gram-positive bacteria (45). It is well established that *S. aureus* secretes factors that interfere with complement activation, mainly by inhibiting the conversion of C3 (46, 47). Our study suggests yet another route of interference with complement deposition and hence the host immune system; the liberation of PGN fragments from the cell wall may serve as decoys, providing protection for the *S. aureus* cell through futile conversion of C3. The classical pathway dominates the complement consumption measured in our assays, consistent with the topology of the liberated PGN fragments, which apparently are being ideally shaped to support complement activation through the binding of IgM. IgM supports the most powerful route of complement activation, and the subversion of this mechanism by *S. aureus* and potentially other Gram-positive pathogens through release of PGN fragments could consequently be a significant contribution to their virulence.

Acknowledgments

We thank Lone Lysgaard, Tove Findahl, and Bettina W. Grumsen for excellent technical assistance. We thank Drs. Peter Kingshott and Duncan Sutherland for helpful discussions on the application of nanoparticles and Dr. Niels Trolle Andersen for advice on the statistical analysis. Dr. Søren Ladefoged kindly provided information on the C3 concentration in serum. We thank Dr. Jan Skov Pedersen for helpful comments on the application of DLS and Drs. Steffen Thiel and Jens Chr. Jensenius for several helpful discussions and suggestions. Dr. Malcolm W. Turner also kindly assisted with the revision of this manuscript.

Disclosures

The authors have no financial conflicts of interest.

References

1. Sjöberg, A. P., L. A. Trouw, and A. M. Blom. 2009. Complement activation and inhibition: a delicate balance. *Trends Immunol.* 30: 83–90.
2. Dong, M., S. Xu, C. L. Oliveira, J. S. Pedersen, S. Thiel, F. Besenbacher, and T. Vorup-Jensen. 2007. Conformational changes in mannan-binding lectin bound to ligand surfaces. *J. Immunol.* 178: 3016–3022.
3. Wallis, R. 2007. Interactions between mannose-binding lectin and MASPs during complement activation by the lectin pathway. *Immunobiology* 212: 289–299.
4. Gaboriaud, C., N. M. Thielens, L. A. Gregory, V. Rossi, J. C. Fontecilla-Camps, and G. J. Arlaud. 2004. Structure and activation of the C1 complex of complement: unraveling the puzzle. *Trends Immunol.* 25: 368v373.
5. Gros, P., F. J. Milder, and B. J. Janssen. 2008. Complement driven by conformational changes. *Nat. Rev. Immunol.* 8: 48–58.
6. Lo Conte, L., C. Chothia, and J. Janin. 1999. The atomic structure of protein-protein recognition sites. *J. Mol. Biol.* 285: 2177–2198.
7. Perkins, S. J., A. S. Nealis, B. J. Sutton, and A. Feinstein. 1991. Solution structure of human and mouse immunoglobulin M by synchrotron X-ray scattering and molecular graphics modelling. A possible mechanism for complement activation. *J. Mol. Biol.* 221: 1345–1366.
8. Roux, K. H. 1999. Immunoglobulin structure and function as revealed by electron microscopy. *Int. Arch. Allergy Immunol.* 120: 85–99.
9. Feinstein, A., E. A. Munn, and N. E. Richardson. 1971. The three-dimensional conformation of M and A globulin molecules. *Ann. N. Y. Acad. Sci.* 190: 104–121.
10. Feinstein, A., and E. A. Munn. 1969. Conformation of the free and antigen-bound IgM antibody molecules. *Nature* 224: 1307–1309.
11. Carballido-López, R., and A. Formstone. 2007. Shape determination in *Bacillus subtilis*. *Curr. Opin. Microbiol.* 10: 611–616.
12. Giesbrecht, P., T. Kersten, H. Maidhof, and J. Wecke. 1998. Staphylococcal cell wall: morphogenesis and fatal variations in the presence of penicillin. *Microbiol. Mol. Biol. Rev.* 62: 1371–1414.
13. Cloud-Hansen, K. A., S. B. Peterson, E. V. Stabb, W. E. Goldman, M. J. McFall-Ngai, and J. Handelsman. 2006. Breaching the great wall: peptidoglycan and microbial interactions. *Nat. Rev. Microbiol.* 4: 710–716.
14. Pamer, E. G. 2007. Immune responses to commensal and environmental microbes. *Nat. Immunol.* 8: 1173–1178.
15. Wilkinson, B. J., Y. Kim, and P. K. Peterson. 1981. Factors affecting complement activation by *Staphylococcus aureus* cell walls, their components, and mutants altered in teichoic acid. *Infect. Immun.* 32: 216–224.
16. Pinegin, B. V., A. V. Kulakov, E. A. Makarov, P. W. Ledger, and R. M. Khaitov. 1995. The occurrence of natural antibodies to minimal component of bacterial cell wall (N-acetylglucosaminyl-N-acetylmuramyl dipeptide) in sera from healthy humans. *Immunol. Lett.* 47: 33–37.
17. Spitznagel, J. K., K. J. Goodrum, D. J. Warejcka, J. L. Weaver, H. L. Miller, and L. Babcock. 1986. Modulation of complement fixation and the phlogistic capacity of group A, B, and D streptococci by human lysozyme acting on their cell walls. *Infect. Immun.* 52: 803–811.
18. Thiel, S., M. Møller-Kristensen, L. Jensen, and J. C. Jensenius. 2002. Assays for the functional activity of the mannan-binding lectin pathway of complement activation. *Immunobiology* 205: 446–454.
19. Coligan, J. E., B. E. Bierer, D. H. Margulies, E. M. Shevach, and W. Stober, eds 2005. *Current Protocols in Immunology*. John Wiley & Sons, Inc., New York.
20. Platts-Mills, T. A., and K. Ishizaka. 1974. Activation of the alternate pathway of human complements by rabbit cells. *J. Immunol.* 113: 348–358.
21. Czop, J. K., and K. F. Austen. 1985. Properties of glycans that activate the human alternative complement pathway and interact with the human monocyte beta-glucan receptor. *J. Immunol.* 135: 3388–3393.
22. Brown, W. 1993. *Dynamic Light Scattering:The Method and Some Applications*. Clarendon Press, Oxford.
23. Anastase, S., D. Letourneur, and J. Jozefonvicz. 1996. Affinity chromatography of human anti-dextran antibodies. Isolation of two distinct populations. *J. Chromatogr. B Biomed. Appl.* 686: 141–150.
24. Karakawa, W. F., and W. F. Vann. 1982. *Capsular Polysaccharides of Staphylococcus aureus*. Thieme Stratton Inc., New York.
25. Skov Sørensen, U. B., J. Blom, A. Birch-Andersen, and J. Henrichsen. 1988. Ultrastructural localization of capsules, cell wall polysaccharide, cell wall proteins, and F antigen in pneumococci. *Infect. Immun.* 56: 1890–1896.
26. Edwards, C. H., and D. E. Penney. 2006. *Calculus*. Prentice-Hall International, Inc., Englewood Cliffs, NJ.
27. Stewart, J. 2007. *Calculus*. Brooks Cole, Pacific Grove, CA.
28. Al-Hanbali, O., K. J. Rutt, D. K. Sarker, A. C. Hunter, and S. M. Moghimi. 2006. Concentration dependent structural ordering of poloxamine 908 on polystyrene nanoparticles and their modulatory role on complement consumption. *J. Nanosci. Nanotechnol.* 6: 3126–3133.
29. Moghimi, S. M., A. C. Hunter, C. M. Dadswell, S. Savay, C. R. Alving, and J. Szebeni. 2004. Causative factors behind poloxamer 188 (Pluronic F68, Flocor)-induced complement activation in human sera. A protective role against poloxamer-mediated complement activation by elevated serum lipoprotein levels. *Biochim. Biophys. Acta* 1689: 103–113.
30. Vonarbourg, A., C. Passirani, P. Saulnier, and J. P. Benoit. 2006. Parameters influencing the stealthiness of colloidal drug delivery systems. *Biomaterials* 27: 4356–4373.
31. Lind, K., M. Kresse, N. P. Debus, and R. H. Müller. 2002. A novel formulation for superparamagnetic iron oxide (SPIO) particles enhancing MR lymphography: comparison of physicochemical properties and the in vivo behaviour. *J. Drug Target.* 10: 221–230.
32. Burger, R., G. Zilow, A. Bader, A. Friedlein, and W. Naser. 1988. The C terminus of the anaphylatoxin C3a generated upon complement activation represents a neoantigenic determinant with diagnostic potential. *J. Immunol.* 141: 553–558.
33. Vorup-Jensen, T., E. S. Sørensen, U. B. Jensen, W. Schwaeble, T. Kawasaki, Y. Ma, K. Uemura, N. Wakamiya, Y. Suzuki, T. G. Jensen, et al. 2001. Recombinant expression of human mannan-binding lectin. *Int. Immunopharmacol.* 1: 677–687.
34. Scheffers, D. J., and M. G. Pinho. 2005. Bacterial cell wall synthesis: new insights from localization studies. *Microbiol. Mol. Biol. Rev.* 69: 585–607.
35. Borsos, T., and H. J. Rapp. 1965. Hemolysin titration based on fixation of the activated first component of complement: evidence that one molecule of hemolysin suffices to sensitize an erythrocyte. *J. Immunol.* 95: 559–566.
36. Simberg, D., J. H. Park, P. P. Karmali, W. M. Zhang, S. Merkulov, K. McCrae, S. N. Bhatia, M. Sailor, and E. Ruoslahti. 2009. Differential proteomics analysis of the surface heterogeneity of dextran iron oxide nanoparticles and the implications for their in vivo clearance. *Biomaterials* 30: 3926–3933.
37. Janssen, B. J., A. Christodoulidou, A. McCarthy, J. D. Lambris, and P. Gros. 2006. Structure of C3b reveals conformational changes that underlie complement activity. *Nature* 444: 213–216.
38. Janssen, B. J., R. J. Read, A. T. Brünger, and P. Gros. 2007. Crystallography: crystallographic evidence for deviating C3b structure. *Nature* 448: E1–E2, discussion E2–E3.
39. Pangburn, M. K., R. D. Schreiber, and H. J. Müller-Eberhard. 1983. C3b deposition during activation of the alternative complement pathway and the effect of deposition on the activating surface. *J. Immunol.* 131: 1930–1935.
40. Schuhardt, V. T., T. W. Huber, and L. M. Pope. 1969. Electron microscopy and viability of lysostaphin-induced staphylococcal spheroplasts, protoplast-like bodies, and protoplasts. *J. Bacteriol.* 97: 396–401.
41. Beveridge, T. J. 1981. Ultrastructure, chemistry, and function of the bacterial wall. *Int. Rev. Cytol.* 72: 229–317.
42. Touhami, A., M. H. Jericho, and T. J. Beveridge. 2004. Atomic force microscopy of cell growth and division in *Staphylococcus aureus*. *J. Bacteriol.* 186: 3286–3295.
43. Park, J. T., and T. Uehara. 2008. How bacteria consume their own exoskeletons (turnover and recycling of cell wall peptidoglycan). *Microbiol. Mol. Biol. Rev.* 72: 211–227.
44. Cloud-Hansen, K. A., K. T. Hackett, D. L. Garcia, and J. P. Dillard. 2008. *Neisseria* gonorrhoeae uses two lytic transglycosylases to produce cytotoxic peptidoglycan monomers. *J. Bacteriol.* 190: 5989–5994.
45. Vance, R. E., R. R. Isberg, and D. A. Portnoy. 2009. Patterns of pathogenesis: discrimination of pathogenic and nonpathogenic microbes by the innate immune system. *Cell Host Microbe* 6: 10–21.
46. Nizet, V. 2007. Understanding how leading bacterial pathogens subvert innate immunity to reveal novel therapeutic targets. *J. Allergy Clin. Immunol.* 120: 13–22.
47. Blom, A. M., T. Hallström, and K. Riesbeck. 2009. Complement evasion strategies of pathogens-acquisition of inhibitors and beyond. *Mol. Immunol.* 46: 2808–2817.
48. Pettersen, E. F., T. D. Goddard, C. C. Huang, G. S. Couch, D. M. Greenblatt, E. C. Meng, and T. E. Ferrin. 2004. UCSF Chimera—a visualization system for exploratory research and analysis. *J. Comput. Chem.* 25: 1605–1612.